T cells specific for α-myosin drive immunotherapy related myocarditis

Margaret L. Axelrod[1], **Wouter C. Meijers**[1,2], **Elles M. Screever**[1,2], **Juan Qin**[1,3], **Mary Grace Carroll**[1], **Xiaopeng Sun**[1], **Elie Tannous**[1], **Yueli Zhang**[1], **Ayaka Sugiura**[1], **Brandie C. Taylor**[1], **Ann Hanna**[1], **Shaoyi Zhang**[3], **Kaushik Amancherla**[1], **Warren Tai**[1,4], **Jordan J. Wright**[1], **Spencer C. Wei**[5], **Susan R. Opalenik**[1], **Abigail L. Toren**[1], **Jeffrey C. Rathmell**[6,7,8], **P. Brent Ferrell**[1], **Elizabeth J. Phillips**[1], **Simon Mallal**[1], **Douglas B. Johnson**[1,7], **James P. Allison**[5,9], **Javid J. Moslehi**[*,1,3], **Justin M. Balko**[*,1,6,7]

[1]Department of Medicine, Vanderbilt University Medical Center, Nashville, TN, 37232, USA

[2]Department of Cardiology, University Medical Center Groningen, Groningen, The Netherlands

[3]Section of Cardio-Oncology & Immunology, Division of Cardiology and the Cardiovascular Research Institute, University of California San Francisco, 555 Mission Bay Blvd South, Box 3118, San Francisco, CA 94143-3118, USA

[4]Division of Cardiology, University of California, Los Angeles, CA, 90095, USA

[5]Department of Immunology, The University of Texas MD Anderson Cancer Center, Houston, TX, 77030, USA

[6]Department of Pathology, Microbiology and Immunology, Vanderbilt University Medical Center, Nashville, TN, 37232, USA

[7]Vanderbilt-Ingram Cancer Center, Vanderbilt University Medical Center, Nashville, TN, 37232, USA

[8]Vanderbilt Center for Immunobiology, Vanderbilt University Medical Center, Nashville, TN, 37232, USA

[9]Parker Institute for Cancer Immunotherapy, The University of Texas MD Anderson Cancer Center, Houston, TX, 77030, USA

Abstract

Immune-related adverse events, particularly severe toxicities such as myocarditis (MC), are major challenges to immune checkpoint inhibitor (ICI) utility in anti-cancer therapy[1]. The pathogenesis of ICI-myocarditis (ICI-MC) is poorly understood. *Pdcd1−/−Ctla4+/−* mice recapitulate clinicopathologic features of ICI-MC, including myocardial T cell infiltration[2]. Single cell RNA/T cell receptor (TCR) sequencing on the cardiac immune infiltrate of *Pdcd1−/−Ctla4+/−* mice identified clonal effector CD8+ T cells as the dominant cell population. Treatment with anti-CD8, but not anti-CD4, depleting antibodies rescued survival of *Pdcd1−/−Ctla4+/−* mice. Adoptive transfer of immune cells from mice with MC induced fatal MC in recipients which required CD8+ T cells. α -myosin, a cardiac specific protein absent from the thymus[3,4], was identified as the cognate antigen source for three MHC-I restricted TCRs derived from mice with fulminant MC. Peripheral blood T cells from three patients with ICI-MC were expanded by α-myosin peptides, and these α-myosin expanded T cells shared TCR clonotypes with diseased heart and skeletal muscles, indicating that α-myosin may be a clinically important autoantigen in ICI-MC. These studies underscore the critical role for cytotoxic CD8+ T cells, are the first to identify a candidate autoantigen in ICI-MC and yield new insights into ICI toxicity pathogenesis.

Immune checkpoint inhibitors (ICIs) have drastically altered the treatment landscape and prognosis for many cancers. However, not all patients respond to treatment and many experience immune-related adverse events (irAEs), especially when ICIs are used in combination. Thus, preventing, diagnosing, and treating irAEs are urgent clinical challenges. Currently, clinically actionable biomarkers of response and toxicity are limited and the mechanistic basis of irAEs is poorly defined.

Myocarditis (MC) is an uncommon irAE, affecting <1% of ICI-treated patients, but has a mortality rate of nearly 50%[1,5]. Combination ICI therapy (with anti-PD-1 and anti-CTLA4) is the most well-established risk factor for ICI-myocarditis (ICI-MC)[6-9]. ICI-

MC is pathologically characterized by predominance of T lymphocytes and macrophages in the heart and often co-occurs with myositis, with early studies suggesting common clonotypes of T lymphocytes in both tissues[5]. These data suggest the possibility of shared target antigens driving T lymphocyte expansion and activation, which would be critical for pathogenesis; however, experimental data have been lacking.

Generally, mice treated with ICIs do not replicate the full spectrum of irAEs seen in patients, limiting research on mechanisms of toxicity. We recently described a mouse model of ICI-MC in which C57BL6/J mice with homozygous knockout of *Pdcd1* and heterozygous deletion of *Ctla4* die prematurely and specifically due to MC, recapitulating clinical and pathological features of ICI-MC[2]. Severe inflammation is specific to the heart in these mice. By flow cytometry, the myocardial immune infiltrate is primarily composed of CD8+ T cells, similar to patients with ICI-MC. Furthermore, treatment with abatacept, a CTLA4 fusion protein, attenuates MC and increases survival in the mice, consistent with early clinical data from patients with ICI-MC treated with abatacept[2,10]. Here we utilize this mouse model of ICI-MC to characterize the immune infiltrates, establish CD8+ T cells as necessary for disease, and identify α-myosin as a cognate antigen for the most abundant TCRs in MC. Furthermore, we extend these findings to human disease and find that α-myosin expanded TCRs are present in inflamed cardiac and skeletal muscles in patients with ICI-MC.

Cardiac clonal CD8+ T cells are abundant

Fulminant MC affects 50% of *Pdcd1−/−Ctla4+/−* mice and was characterized by histologic destruction of the myocardial architecture (Fig. 1a, b)[2]. Incidence was higher in female mice, in line with data in patients that female sex is a risk factor for ICI-MC[2,9]. The myocardial immune infiltrate in affected mice was primarily composed of CD8+ T cells and did not differ by sex (Extended Data Fig. 1a)[2]. No significant antibody deposits or B220+ B cells were observed in the hearts of mice with MC, supporting further study of T cells at the site of disease (Extended Data Fig. 1b). We used single cell RNA and TCR sequencing to characterize sorted CD45+ infiltrating immune cells from six healthy wild type mouse hearts and four hearts from *Pdcd1−/−Ctla4+/−* mice affected by MC. Dimensionality reduction with uniform manifold approximation and projection (UMAP), clustering with Louvain and cluster cell type annotation assisted by SingleR showed distinct immune cell populations in MC compared to control (Fig. 1c; Extended Data Fig. 2a). The largest difference was seen in the activated T cell cluster, which made up 34% of the MC immune cells, and only 2% of the control immune cells. Markers of activation such as *Ccl5, Ccl4, Tigit, Nkg7,* and *Gzmb* were upregulated in the T cell clusters in MC compared to control T cell clusters (Extended Data Fig. 2b). Conversely, markers of naïve status such as *Ccr7, Lef1* and *Sell* were upregulated in control T cells. Activation markers were also upregulated in other clusters, including myeloid cell subsets, in the MC samples (Extended Data Fig. 2c). *Aw112010*, a long noncoding RNA essential for the orchestration of mucosal immunity during infections and in colitis, was strongly upregulated in several clusters in the MC samples[11,12]. In contrast, B lymphocytes made up most of the immune cells in the control heart, consistent with previous studies[13-15].

To further characterize T lymphocytes, we performed dimensionality reduction and clustering on *Cd3e+* and TCR+ cells, which showed differential cluster abundance in MC compared to control (Fig. 1d). Differential gene expression analyses and plotting of key identity genes revealed distinct cluster identities (Fig. 1e; Extended Data Fig. 3a). Cluster 0 cells were activated effector CD8+ T cells expressing *Gzmb, Ifng,* and *Nkg7.* Cluster 1 cells were resting CD8+ T cells, expressing *Ccr7, Sell,* and *Klf2.* Cluster 2 cells were CD4+ T cells expressing *Cd4, Ccr7,* and *Cd40lg.* Cluster 3 cells were proliferative CD8+ T cells expressing *Mki67, Cdk1* and *Tk1.* Cluster 4 cells were *Cd24a* expressing T cells and comprised a small fraction of the total T cells. CD24 is upregulated with TCR signaling and is necessary for T cell proliferative capacity[16,17]. Cluster 0 (effector CD8+ T cells) comprised the majority of the MC cells. Cluster 3 (proliferating CD8+ T cells) and cluster 0 were enriched in the MC sample relative to the control sample. Cluster 0 and cluster 3 also had the highest TCR density, defined as the number of neighboring cells with the same TCR α and β chain. High TCR density was limited to the MC sample (Fig. 1f). Genes upregulated in cluster 0 T cells included *Ccl5, Nkg7, Ccl4, Cxcr6, Lag3,* and *Prf1* (Fig. 1g; Extended Data Fig. 3b). We also sought to investigate genes associated with tissue residency, as intravascular immune cells were not excluded in our tissue preparation protocol. We found substantial expression of *Cd69, Itgb1, Itgal, Cxcr3, Cxcr6,* and *Runx3* in MC T cell clusters, and lower levels of these genes in control T cells (Extended Data Fig. 3c)[18,19]. These data suggest that MC T cells were CD8+, tissue-resident, [15]effector and proliferating.

We next sought to assess the clonality of TCRs in the MC samples using both bulk and single cell TCR sequencing. Cardiac tissue from affected *Pdcd1−/−Ctla4+/−* mice had lower Shannon diversity than splenic tissue from healthy wild type mice or mice with MC, indicating a higher degree of clonal TCRs (Extended Data Fig. 3d), which did not differ by sex. No clonal (>2 cells with the same TCR clonotype) cells were identified by single cell TCR sequencing of healthy cardiac immune infiltrate. In contrast, 63% of TCR+ cells in the MC samples represented clonal TCRs (Extended Data Fig. 3e). Comparing gene expression by clonality showed that non-clonal cells from control samples expressed *Cd8a*, *Cd4*, and markers associated with naïve status, rather than activation. In contrast, clonal cells from MC samples expressed *Cd8a* and cytotoxicity genes such as *Nkg7* and *Gzmb,* but not *Cd4* or markers of naïve status (Fig. 1h). These data show that there was a large population of highly activated, clonally expanded CD8+ T cells in murine ICI-MC.

CD8+ T cells are necessary for myocarditis

Early administration of corticosteroids, which are immunosuppressive through a variety of mechanisms, is associated with better survival in patients with ICI-MC, but severe cases can be refractory to steroids[20,21]. In our murine model, dexamethasone treatment did not attenuate MC or extend survival, consistent with a severe phenotype (Extended Data Fig. 4a). Using anti-CD8 and anti-CD4 depleting antibodies (starting at 21 days of age and administered three times weekly, confirmation shown in Extended Data Fig. 4b), we tested whether depletion of these cell subsets would attenuate MC and affect survival of *Pdcd1−/ −Ctla4+/−* mice. Depletion of CD8+ cells, but not CD4+ cells, significantly rescued survival in these mice (Fig. 2a). Corroborating these data, adoptive transfer of whole splenocytes, but not splenocytes from which CD8+ cells were depleted (confirmed in Extended Data

Fig. 4c), from *Pdcd1−/−Ctla4+/−* mice with MC to *Rag1−/−* recipients was sufficient to induce fatal MC (Fig. 2b-c). The single fatality in the CD8-depleted arm was likely due to a bowel obstruction with no evidence of MC histologically. Immunohistochemistry showed abundant cardiac infiltration of CD3+ and CD8+ cells, and limited CD4+ cells and F4/80+ cells, in the whole splenocyte recipients but not the CD8-depleted recipients (Fig. 2d; Extended Data Fig. 4d). We performed TCR β chain sequencing on the cardiac tissue of one donor mouse (Donor) and four whole splenocyte recipients (Rec1, Rec2, Rec3, and Rec4; Fig. 2e). High numbers (>2000) of TCR reads were seen in all sequenced hearts, indicating significant T cell infiltration, as expected from histology (Extended Data Fig. 4e). In 4/4 recipient mice, the most clonal TCR β chain occupied greater than 65% of the total cardiac TCR repertoire, indicating strong monoclonal expansion. The most clonal TCR β chain (CDR3: CASSLRRGEQYF) in the donor heart (which comprised 37% of the donor cardiac repertoire) was expanded in three of four recipients (Rec1, 3, 4). Interestingly, in one recipient mouse (Rec2), a low frequency TCR from the donor was expanded and occupied the majority of the TCR β chain repertoire (CDR3: CASSLGGTVQDTQYF). This high degree of expansion from donor to recipient cardiac tissue suggests a single TCR clonotype may drive MC in the recipient animals. Together, these results strongly indicated that CD8+ T lymphocytes are necessary for the development of MC.

Myocarditis TCRs recognize α-myosin

Next, we aimed to identify the cognate antigen for clonal murine TCRs. For antigen discovery, we tested five TCRs derived from single cell RNA/TCR sequencing and selected on the basis of their abundance. These TCRs (TCR-A and TCRs 1-4) were primarily associated with cluster 0 effector CD8+ T cells and cluster 3 proliferating T cells (Fig. 3a). We also included two TCRs which were expanded the hearts of recipient mice in adoptive transfer experiments (TCRs B and C). TCR-B was the most abundant TCR in the heart of the donor and three recipients (β CDR3: CASSLRRGEQYF). TCR-C was the most abundant TCR in the heart of recipient 2 (β CDR3: CASSLGGTVQDTQYF; Fig. 2e). CDR3 amino acid sequences, V genes, and J genes are shown in Table 1. These TCRs were reconstructed using Stitchr, cloned, and retrovirally transduced into Jurkat nuclear factor of activated T cells (NFAT)-GFP reporter cells[22-24]. Syngeneic bone marrow derived dendritic cells were used as antigen presenting cells (APCs).

We used a candidate autoantigen approach for TCR screening. Analysis of published RNA sequencing data on thymic APCs showed four cardiac enriched genes (genes where expression in the heart was significantly enriched relative to other tissues) with no detectable expression in the thymus (*MYH6, NPPA, NPPB, SBK2;* Fig. 3b)[4]. Lack of thymic expression would be predicted to enable self-reactive T cells to escape negative selection, an important mechanism of self-tolerance. Expression of these genes was also low to absent in the thymus of *Pdcd1−/−Ctla4+/−* mice and did not differ by sex (Extended Data Fig.5a). We used a library of 172 overlapping peptides, covering all of α-myosin (encoded by *Myh6*), ANP (encoded by *Nppa*), BNP (encoded by *Nppb*) and SBK2 (encoded by *Sbk2*; Extended Data Table 1). Three TCR cell lines, including both expanded TCRs (B and C), had NFAT activity in response to α-myosin peptides. None of the other three tested cardiac proteins activated any of the TCR cell lines (Fig. 3c). *MYH6* (α-myosin) has been confirmed by

other groups to not be expressed in the thymus in mice or humans and has been shown to be an MHC-II restricted autoantigen in mouse models[3,25,26]. Interestingly, 4/5 single cell-derived TCR cell lines did not recognize any of the tested cardiac peptides (denoted TCRs 1-4 to differentiate from TCRs A-C where cognate antigens were identified). These data suggest two important possibilities: 1) the presence of "bystander" T cells which are attracted to the site of inflammation but are not specific for disease-causing antigens or 2) the possibility that these TCRs might recognize other cardiac antigens which are important in disease pathogenesis. The bystander TCR hypothesis is well supported by prior literature in tumor immunology showing that a minority of tumor-infiltrating T cells are likely to be tumor specific[27-31].

TCRs A and B activated NFAT reporters in response to the same α-myosin peptide (MYH6$_{181-200}$), whereas TCR-C had NFAT activity against a distinct α-myosin peptide (MYH6$_{406-425}$; Fig. 3c). From these 20 amino acid peptides, we used TepiTool to identify the most likely immunogenic epitopes[32] and re-screened these epitopes against the reporter TCR lines. TCRs A and B recognized MYH6$_{191-198}$ (VIQYFASI), while TCR-C recognized MYH6$_{418-425}$ (VQQVYYSI; Fig. 3d). VIQYFASI and VQQVYYSI both had strong predicted binding to H2-Kb (Extended Data Table 2). The tyrosine and phenylalanine residues at position five of the peptides are known to be key binding epitopes for H2-Kb[33]. In line with these predictions, antibody blocking of H2-Kb, but not H2-Db, abrogated NFAT reporter activity for all three cell lines (Fig. 3e). Using an empty H2-Kb tetramer loaded with either VIQYFASI or VQQVYYSI, compared to a tetramer loaded with an irrelevant peptide (SIINFEKL), we found that 6-30% of the cardiac infiltrating CD8+ T cells were specific for one of the two α-myosin peptides in nine additional *Pdcd1−/−Ctla4+/−* mice with MC (Fig. 3f,g; Extended Data Fig. 5b). We did not identify any mice with MC lacking VIQYFASI or VQQVYYSI tetramer positive CD8+ T cells in their hearts, demonstrating the ubiquity of α-myosin reactive T cells in this murine model. Notably, high levels of α-myosin tetramer positive CD8+ T cells were confined to the hearts (Extended Data Fig. 5c). These data strongly suggest that α-myosin is an important MHC-I restricted autoantigen in murine immune checkpoint deficiency MC.

α-myosin TCRs are found in ICI-MC patients

We next aimed to test the relevance of α-myosin as a potential autoantigen in humans, using three healthy donors and three patients with histologically-proven fulminant ICI-MC. ICI-MC patient information is summarized in Table 2. First, we tested whether it was possible to expand α-myosin specific T cells from peripheral blood mononuclear cells (PBMCs). PBMCs were stimulated with α-myosin peptides or control cytomegalovirus, Epstein-Barr virus and influenza (CEF) peptides (in healthy donor PBMCs only) for 14 days to generate expanded PBMCs (exPBMC). TCR β chain sequencing was used to assess expansion. Shannon diversity decreased from pre-expansion PBMC to α-myosin exPBMC for healthy donors and ICI-MC patients, indicating clonal expansion of α-myosin specific T cells. Interestingly, Shannon diversity did not change from baseline to CEF peptide expansion, suggesting that α-myosin is a strong stimulus for clonal T cell expansion (Fig. 4a). For all donors, both α-myosin and CEF stimulation resulted in expansion of some individual TCR clonotypes. This expansion can be seen by comparing the frequency of each TCR β chain

in the baseline PBMC compared to the exPBMC of the same patient (Extended Data Fig. 6a, b). These data suggest that both healthy donors and ICI-MC patients have peripheral α-myosin specific T cells capable of expansion in certain conditions.

To assess whether α-myosin expanded TCR clones might be involved in cardiac and skeletal muscle toxicity, we compared TCR β chain repertoires in the heart and inflamed muscle to those overrepresented in α-myosin exPBMC relative to unexpanded PBMC. We performed bulk TCR β chain sequencing on formalin-fixed paraffin embedded tissues from endomyocardial biopsy (patient 1 and 3) and autopsy material (patients 1 and 2). Tissue samples from each MC patient are summarized in Fig. 4b. High numbers of total TCR reads (>1500) were obtained in all samples, consistent with high T cell infiltration (Extended Data Fig. 6c). Shannon diversity was lower in the hearts and skeletal muscles of patients with ICI-MC compared to inflamed colonic tissue of patients with ICI-colitis or Crohn's disease, indicating the high clonality of TCR repertoires seen in ICI-MC compared to another highly T cell infiltrated immunotherapy toxicity[34] (Fig. 4a). Biopsy samples of acute cellular rejection following cardiac transplantation were also included as cardiac-specific comparison TCR repertoires. These samples had low Shannon diversity, consistent with T cell-mediated anti-cardiac autoimmunity (Fig. 4a).

Plotting the degree of α-myosin expansion (count in α-myosin exPBMC minus count in pre-expansion PBMC, with expansion shown in red) against the abundance of the same TCR β chain in the autologous inflamed tissues of ICI-MC patients, shows that α-myosin expanded TCRs are present in inflamed hearts from all three patients (Fig. 4c; Extended Data Fig. 8a). Some α-myosin expanded TCRs were abundant in the inflamed heart and skeletal muscles (Fig. 4c; Extended Data Fig. 7), suggesting that α-myosin may be a relevant disease antigen for ICI-MC and myositis. We performed single cell RNA/TCR sequencing on the sorted CD3+ exPBMC from patient 1. Gene expression analysis of TCR+ cells showed expression of *CD3E* in all cells (including both *CD8A* and *CD4* expressing cells), and a very small population of residual *CD79A* expressing B cells (Extended Data Fig. 8a). We further filtered cells based on a shared TCR β chain with the cardiac TCR repertoire (overlap with bulk β chain sequencing) which would be expected to be enriched for disease-relevant TCRs. Following dimensionality reduction with UMAP, the cells clustered distinctly by group (Fig. 4d). Of the cells with TCR clonotypes shared with the heart, a significantly higher proportion were clonal in the exPBMC relative to cells with TCRs not present in the heart (Fig. 4e) and these clonal cells had high expression of *CD8A* (Fig. 4f; Extended Data Fig. 8b). Clonal cells in the exPBMC are expected to be enriched for α-myosin specificity. Clonal cells with TCRs present in the heart also have high expression of markers of activation such as *NKG7*, *GZMB*, and *GNLY* (Fig. 4f; Extended Data Fig. 8b).

To confirm that α-myosin expansion generates clonal TCRs specific for α-myosin, we aimed to map the epitope specificity and MHC restriction of a TCR found in both the exPBMC and cardiac tissue of patient 1 (TCR-Pt1; Extended Data Fig. 9a). HLA types for ICI-MC patients and healthy donors are shown in Extended Data Table 3. We reconstructed and transduced TCR-Pt1 into Jurkat NFAT-GFP reporter cells (TCR CDR3 and gene information is shown in Table 1). Using the same approach as for murine TCR cell lines of testing against the α-myosin 20 amino acid peptide library, followed by TepiTool-

guided epitope narrowing, we found that TCR-Pt1 activated the NFAT reporter specifically to MYH6$_{443-451}$ (RINATLETK; Fig. 4g). This peptide has strong predicted binding to HLA-A*03:01 using TepiTools. In line with this prediction, the TCR-Pt1 cell line stained with a tetramer with MYH6$_{443-451}$ loaded on HLA-A*03:01 but not a tetramer with the same peptide loaded on HLA-A*24:02 (Extended Data Fig. 9b). Pt1 carries both of these HLA-A alleles. We next tested the MYH6$_{443-451}$ on A*03:01 tetramer against exPBMC of healthy donors and ICI-MC patients carrying HLA-A*03:01. We found high prevalence of MYH6$_{443-451}$ specific T cells in the exPBMC of ICI-MC patient 1 and two healthy donors and low but detectable MYH6$_{443-451}$ specific T cells in the exPBMC of ICI-MC patient 3 (Fig. 4h,i; Extended Data Fig. 9c). Patient 2 was not assessed because they lacked the HLA-A*03:01 allele. Thus, CD8+ cytotoxic T cells specific for α-myosin are present in the blood and diseased hearts of patients with fulminant ICI-MC, and may also be present in healthy individuals.

Tumor-specific *MYH6* expression

The importance of α-myosin as an autoantigen in ICI-MC raises the possibility that tumor cells may aberrantly express *MYH6* and tumor reactive T cells specific for α-myosin epitopes may develop and lead to an increased risk for ICI-MC. It has been previously published by our group that a patient with fulminant ICI-MC had aberrant melanoma-specific expression of muscle transcripts, including *MYH6*[5]. Using a previously published dataset of RNA sequencing on melanoma tumors treated with ICI, we found that 37/91 tumors expressed low but detectable levels of *MYH6* (Extended Data Fig. 10a)[35]. Despite treatment with ICI, none of these patients developed clinically significant MC or myositis. However, very few patients with *MYH6* expression were treated with combination anti-CTLA4 and anti-PD-1, which is a known risk factor for ICI-MC. Given the rarity of MC and the comparatively low patient numbers examined here, these data are insufficient to determine whether tumor-specific *MYH6* expression may be a risk factor for ICI-MC. HLA type may be an important modifying factor. Importantly, tumor-specific *MYH6* expression is not unique to this dataset. Analysis of The Cancer Genome Atlas (TCGA) melanoma cohort shows that 250 of 363 tumors had detectable *MYH6* expression (Extended Data Fig. 10b).

Discussion

Immunotherapy toxicities are important limitations to the use of ICIs. Here we present a new perspective on ICI-MC as an antigen-driven, cytotoxic T cell mediated toxicity. We used a genetically altered mouse to model a human drug toxicity and found that *Pdcd1−/−Ctla4+/−* mice recapitulate many of the important clinicopathologic features of ICI-MC seen in humans, including severe cardiac inflammation predominately comprised of CD8+ T cells. The mice also have significant conduction abnormalities and preserved ejection fraction[2]. Pharmacologic animal models have not replicated these important features. MRL mice treated with anti-PD-1 and anti-CTLA-4 for 8 weeks develop a mild MC that is only evident histologically[2]. Monkeys treated with anti-PD-1 and anti-CTLA-4 develop mild to moderate inflammation in all organs examined including the heart, where mild CD4+ T cell infiltration is seen[36].

We show in our mouse model that MC is characterized by cytotoxic CD8+ T cells with highly clonal TCRs, and that CD8+ cells are necessary for the development of MC. Though CD4 depletion did not rescue survival, it is unknown what role CD4+ T cells play, particularly in the initiation of MC, which is more difficult to determine in a genetic model and is a limitation of our study. The CD8 dependence of our model is in contrast to the CD4 dependence of MC seen in *Pdcd1–/–Lag3–/–* mice, raising the possibility of distinct mechanisms of MC with different immune checkpoint deficiencies[37,38]. Three of the most clonal TCRs, derived from independent mice, recognized α-myosin epitopes. Strikingly, α-myosin specific TCRs expanded when transferred to recipient mice and occupied greater than 65% of the highly inflamed cardiac TCR repertoire at the time of death from MC. Lack of thymic expression suggests that α-myosin specific T cells may escape central tolerance mechanisms[3]. α-myosin specific T cells can be expanded from the blood of healthy donors and patients with ICI-MC. This finding, likely not unique to α-myosin, suggests that the presence of α-myosin specific T cells in the periphery is common in humans. Furthermore, we found T cells specific for the exact epitope MYH6$_{443-451}$ on HLA-A*03:01 could be expanded from the blood in all four tested patients with the HLA-A*03:01 allele. It is currently unknown whether particular HLA alleles may be a risk factor for ICI-MC. Several studies have recently examined associations of HLA alleles and response or toxicity to ICI, but more work is needed, particularly for rare toxicities like MC [39-42]. Additionally, the effect of the microbiome on ICI-MC risk is unknown and should be explored in future work[43,44].

α-myosin expanded TCRs overlapped with TCR repertoires in the diseased hearts and skeletal muscle of three patients with ICI-MC. Although presence of shared clones is insufficient to establish causality, these data suggest that α-myosin may be an important autoantigen in ICI-MC. The presence of other high frequency TCRs in the hearts that were not enriched in the α-myosin expanded repertoires could point to other relevant antigens, particularly by the time MC has become severe.

Prior studies have shown α-myosin to be an MHC-II restricted autoantigen in mouse models, primarily using transgenic TCRs or α-myosin vaccination approaches, where α-myosin is used to initiate an immune response[3,45-50]. Our studies are the first to identify MHC-I restricted α-myosin epitopes in a spontaneous murine model of MC which is dependent on CD8+ T cells. Furthermore, to the best of our knowledge, our studies are among the first to identify a candidate autoantigen for an immunotherapy toxicity in humans. We have also identified novel exact TCR-peptide:MHC interactions for three murine TCRs and one human TCR. Knowledge of the most relevant disease antigens may allow for antigen-directed approaches to suppressing inflammation without sacrificing anti-tumor efficacy such as tolerogenic vaccines. Identification of α-myosin as an autoantigen may also guide identification of biomarkers to predict which patients are at higher risk for MC, such as surveillance of peripheral α-myosin reactive T cells or identification of pre-existing autoantibodies.

Methods

Mice.

Pdcd1−/−Ctla4+/− mice were maintained as previously described[2]. Female mice were primarily (but not exclusively) used in these studies due to their higher incidence of myocarditis. *Rag1−/−* mice were purchased from The Jackson Laboratory (#002216)[51]. For the generation of survival curves, events were defined as either death (i.e., mice found dead) or identification of mice requiring euthanasia (e.g., due to lethargy, moribund, dyspnea, weight loss). All mice were housed at Vanderbilt University Medical Center vivarium, an Association for Assessment and Accreditation of Laboratory Animal Care International (AAALAC)–accredited, specific pathogen-free (SPF) animal facility. All experiments were performed in accordance with Vanderbilt University Medical Center Institutional Animal Care and Use Committee (IACUC) guidelines. Mice were on 12-h light–dark cycles which coincided with daylight in Nashville, TN. The mouse housing facility was maintained at 20–25 °C and 30–70% humidity.

Preparation of cardiac dissociates for single-cell RNA/TCR sequencing.

Single-cell suspensions were obtained from murine hearts by mincing followed by enzymatic digestion with 125 U/mL DNase I (Worthington; cat no. LS002138) and 250 U/mL Collagenase 3 (Worthington; cat no. LS004182). Dissociated hearts were filtered through a 30μm filter. Red blood cells were lysed using ACK lysing buffer (KD Medical/MediaTech; cat no. NC0274127). Single-cell suspensions were either used fresh or cryopreserved in 10% DMSO 90% FBS. Prior to sorting, cells were stained with Alex Flour 488 anti-mouse CD45 (BioLegend; clone 30-F11; cat no. 103122, dilution 1:1000) for 20 minutes at 4°C. Following staining and washing with PBS, cells were resuspended in PBS with DAPI (1:20,000). Live CD45+ immune cells were sorted by fluorescence-activated cell sorting on AF488-positive DAPI-negative events. The wildtype control sample consisted of pooled, without hashing, cardiac immune infiltrates from six female animals, in order to obtain sufficient cells as the healthy heart has a low frequency of cardiac immune cells. The myocarditis sample consisted of four inflamed hearts from female *Pdcd1−/−Ctla4+/−* mice. Inflammation was confirmed by flow cytometry for CD45. Only mice with CD45+ cells comprising greater than ten percent of the total single cells were included. Mice ranged from three to six weeks in age. One inflamed heart was run as an individual sample on the 10X Genomics chromium platform. The additional three inflamed hearts were hashed together using Total Seq C reagents according to the manufacturer's instructions (BioLegend: TotalSeq™-C0301 cat# 155861, TotalSeq™-C0302 cat# 155863, TotalSeq™-C0303 cat# 155865).

Single-cell RNA/TCR sequencing.

Each sample (targeting 5,000 – 15,000 cells/sample) was processed for single cell 5' RNA and TCR sequencing utilizing the 10X Chromium system. Libraries were prepared following the manufacturer's protocol. The libraries were sequenced using the NovaSeq 6000 with 150 bp paired end reads. RTA (version 2.4.11; Illumina) was used for base calling and analysis was completed using 10X Genomics Cell Ranger software. Data were analyzed in R using the filtered h5 gene matrices in the Seurat package[52-54]. Briefly, samples were subset to

include cells with greater than 200 but less than 3000 unique transcripts to exclude likely non-cellular RNA reads and doublets. Cells with greater than 15% of reads coming from mitochondrial transcripts were also excluded as likely dying cells. For murine hearts, hash tag oligos were deconvoluted using HTODemux with positive quantile set at 0.85. Samples were downsized so that equivalent numbers of cells originating from healthy wild type or myocarditis *Pdcd1−/−Ctla4+/−* cardiac infiltrating immune cells were included (2509 cells per genotype of origin). Ten clusters were identified using a resolution of 0.4. UMAP was used for dimensionality reduction with 15 nearest neighbors and minimum distance of 0.5. SingleR was used to assist with cell type annotation of clusters. Clonal is defined as more than two cells with the same TCR clonotype (defined by unique combinations of CDR3 regions). T cells were subset on expression of *Cd3e* > 1.5 and presence of a TCR (n=1266 cells). Clustering with the Louvain algorithm at resolution of 0.3 yielded five distinct clusters. Additional subclustering yielded small clusters of <15 cells. Differential gene expression analyses were used to identify clusters. TCR density is defined as the number of the 100 nearest cell neighbors expressing the same TCR clonotype (alpha and beta chain).

T cell receptor sequencing.

TCR sequencing and clonality quantification was assessed in formalin-fixed paraffin embedded (FFPE) or snap frozen samples of murine hearts or spleens. All human samples were derived from FFPE or isolated PBMC. For FFPE, RNA was extracted from 10μm sections using the Promega Maxwell 16 FFPE RNA kits and the manufacturer's protocol. TCRs were sequenced using the TCR Immunoverse all chain assay following the manufacturer's protocol (Invitae/ArcherDX). Sequencing results were evaluated using the Archer Immunoverse analyzer. CDR3 sequences and frequency tables were extracted from the manufacturers' analysis platform and imported into R for analysis using the Immunarch package (https://immunarch.com) in R.

Antibody-mediated depletion and dexamethasone treatment.

Female *Pdcd1−/−Ctla4+/−* mice were randomly assigned to control or dexamethasone treatment at 21 days of age. Mice were treated with 1mg/kg/day of dexamethasone. Experiment was concluded when mice reached 115 days of life. Female *Pdcd1−/−Ctla4+/−* mice were randomly assigned to control, anti-CD8a, or anti-CD4 injections at 21 days of age. Mice were injected intraperitoneally three times a week with 200μg of anti-CD4 (BioXCell, Cat# BE0003-1, clone GK1.5) or anti-CD8 (BioXCell, Cat# BE0061, clone 2.43) depleting antibodies or vehicle, all in a maximum volume of 100μL. Treatment lasted until 90 days of age. Peripheral blood was sampled via tail prick for assessment of depletion efficiency at week 3. In order to detect an anticipated mortality difference of 50% (for control) to 5% (for an intervention which rescues mortality) with an alpha of 0.05 and 80% power, a sample size of 14 animals per group is needed.

Adoptive transfer.

Splenocytes were isolated from *Pdcd1−/−Ctla4+/−* mice with myocarditis by manual dissociation, filtering, and red blood cell lysis. Myocarditis of the donor mice was confirmed by either H&E or dissociation of the heart and flow cytometry for CD45+ immune cells.

A portion of each spleen underwent CD8 depletion using magnetic bead isolation (Miltenyi CD8 (TIL) MicroBeads, Mouse, Cat# 130-116-478). One million whole or CD8 depleted splenocytes were injected into each *Rag1−/−* recipient mouse in 100μL PBS via tail vein injection. Mice were monitored for death or signs of distress. At death or euthanasia, hearts, spleens, livers, lungs, and kidneys were stained by H&E and evaluated microscopically. In order to detect an anticipated mortality difference of 50% (for whole splenocyte transfer) to 1% (for CD8 depleted splenocyte transfer) with an alpha of 0.05 and 80% power, a sample size of 11 animals per group is needed.

Histology and pathology.

Formalin-fixed tissues were processed routinely into paraffin blocks, sectioned at 5μm, and stained with H&E by standard protocols in Vanderbilt University Medical Center's Translational Pathology Shared Resource (TPSR) core laboratory. To further characterize the mononuclear cardiac infiltrates detected by light microscopy, a panel of IHC markers was employed. IHC staining was performed in the TPSR using standard, validated protocols for chromogenic IHC. All steps besides dehydration, clearing, and coverslipping were performed on the Leica Bond-Max IHC autostainer (Leica Biosystems Inc.). Slides were deparaffinized. Antigen retrieval was performed using EDTA (CD markers) or proteinase K (F4/80) or on the Bond Max using their Epitope Retrieval 2 solution for 20 minutes (CD45R and IgG). Slides were incubated with primary antibodies as indicated below. Secondary antibody labeling was performed for all markers except CD3 and IgG by incubating in rabbit anti-rat antibody (BA-4001, Vector Laboratories, Inc.) for 15 minutes at a 1:650 dilution. Immunolabeling by rabbit antibody was visualized using the Bond polymer refine detection system (#DS9800, Leica Biosystems, Inc.). Slides were then dehydrated, cleared, and coverslipped. For primary antibodies, anti-CD3 (Abcam, Ab16669) was used at 1:250 dilution, anti-CD4 (eBioscience, 14–9766–82) was used at 1:1,000 dilution, anti-CD8 (eBioscience, 14–0808–82) was used at 1:1,000 dilution, anti-F4/80 (Novus Biologicals, NB600–404) was used at 1:900 dilution, and anti-CD45R/B220 (cat# 553086, BD Pharmingen, clone RA3-6B2) was used at 1:20,000 dilution. For IgG, slides were placed in the Biotin Blocking System (Ref# x0590, DAKO, Carpinteria, CA) for 10 minutes each. Slides were incubated in biotinylated goat anti-mouse IgG (Cat# BA-9200, Vector Laboratories, Inc., Burlingame, CA) for 15 minutes at a 1:2000 dilution. The Bond Intense R detection system (Cat#DS9263, Leica Biosystems, Buffalo Grove, IL) was used for visualization. IHC quantification is reported as number of positive cells per high power field (40x), averaged over three high power fields per slide. Slide images were obtained using Olympus cellSens Standard v1.17.

RNA preparation and qPCR analysis.

Flash frozen mouse tissue (cardiac ventricle or thymus) was homogenized using a TissueLyser II (Qiagen) for 2 minutes at 30Hz. RNA was harvested from dissociated tissue using the Maxwell 16 automated workstation (Promega) and LEV simplyRNA Tissue Kit (Promega, Cat# AS1280). RNA was then analyzed for concentration by a NanoDrop 2000 (Thermo Fisher Scientific) before cDNA synthesis using SensiFAST cDNA Synthesis Kit (Bioline, Meridian Bioscience, Inc., Catalog BIO-65054) with 1 μg of RNA per sample. cDNA and SsoAdvanced Universal

SYBR Green Supermix (Bio-Rad, Catalog 1725270) were then combined with target-specific primers on a CFX96 Touch Real-Time PCR Detection System (Bio-Rad). The following primer pairs were used: *Sbk2* forward 5'- CTCTGAGCCCAGAAATGCCA-3' reverse 5'- AATGTGTTCCAGGGCAGAGG- 3'; *Nppb* forward 5'- CGTTTGGGCTGTAACGCACTG- 3' reverse 5'- TCACTTCAAAGGTGGTCCCAG-3'; *Nppa* forward 5'- TCTGATGGATTTCAAGAACCTGCT- 3' reverse 5'- ACACACCACAAGGGCTTAGG- 3'; *Myh6* forward 5'- AACCAGAGTTTGAGTGACAGAATG - 3' reverse 5'- ACTCCGTGCGGATGTCAA-3'; *β-actin* forward 5'- ACGGCCAGGTCATCACTATTG- 3' reverse 5'- AGGATTCCATACCCAAGAAGGAA- 3'. Three technical replicates were used for each reaction. Beta-actin was used as the housekeeping gene. Data were analyzed using the delta Ct method in which the number of cycles needed to amplify the gene of interest is normalized to the number of cycles needed to amplify the housekeeping gene.

Flow cytometry for murine cell populations and Jurkat reporter cells.

Samples were run on an Attune NxT Acoustic Focusing Cytometer (Life Technologies). Data were collected using the Attune NxT Software v3.2.1. Analysis was performed in FlowJo v10.6. Gating was first done on forward scatter and side scatter to exclude debris. Doublets were excluded by gating on FSC area versus FSC height. DAPI was used to exclude dead cells from analyses. Antibodies used: CD45-PerCP/Cy5.5 (BioLegend, cat# 103132, clone 30-F11, dilution 1:400), CD3-AF488 (BioLegend, cat# 100210, clone 17A2, dilution 1:200), CD4-APC (BioLegend, cat# 100412, clone GK1.5, dilution 1:100), CD8a-PE/Cy7 (BioLegend, cat# 100722, clone 53-6.7, dilution 1:400), Thy1.1 (BioLegend, cat# 202506, Clone OX-7, dilution 1:1000 for AF488, 1:500 for APC/Cy7) and TCR-beta chain-PE (BioLegend, cat# 109208, Clone H57-597, dilution 1:200).

TCR sequences and cloning.

TCR sequences were generated from CDR3 regions, V genes and J genes using Stitchr[55]. Paired TCR alpha and beta sequences were derived from single cell sequencing or from the adoptive transfer experiments in which pairing of chains could be inferred from bulk sequencing as single alpha and beta chains made up the majority of each repertoire. Alpha genes and beta genes were separated using a T2A sequence. Restriction digest sites were added to either end. Full TCR gene blocks were synthesized as custom orders from Genewiz. Full TCR block sequences can be found in supplemental material. TCR sequences were cloned into MSCV-IRES-Thy1.1 DEST vector. MSCV-IRES-Thy1.1 DEST was a gift from Anjana Rao (Addgene plasmid # 17442; http://n2t.net/addgene:17442 ; RRID:Addgene_17442)[56]. Retrovirus was made using the platA retroviral packaging cell line (Cell BioLabs RV-102). Jurkat-TCR-ko-CD8+-NFAT-GFP reporter cells were a gift from Dr. Peter Steinberger. Reporter cells were retrovirally transduced with TCRs of interest. TCR expression was confirmed via flow cytometry for Thy1.1 and TCR-beta chain. Retrovirally transduced cells were sorted on the WOLF cell sorter (NanoCellect) for Thy1.1-AF488. Cells were confirmed to be >90% Thy1.1 positive post-sort prior to use in downstream assays.

Antigen discovery.

Jurkat-NFAT-GFP cell lines with reconstructed TCRs were used for antigen screening. Syngeneic (derived from C57BL6 mice) bone marrow derived dendritic cells (BMDCs) were used as APCs. BMDCs were generated by flushing femurs and tibias from mice with PBS, filtering the cells though a 70μM filter, lysing RBCs, and plating in RMPI + 10% FBS + 1% HEPES + 20ng/mL GM-CSF (ProSpec Cat# CYT-222). BMDCs were polarized in GM-CSF containing media for 9 days (replacing the media at days 3 and 6) prior to harvesting the adherent fraction via mechanical dissociation using a cell scrapper and cryopreservation for future experiments. For antigen discovery, BMDCs were thawed into GM-CSF containing media in flat bottom plates the day before adding TCR cell lines and peptides. Cells were plated at a ratio of 1 TCR cell to 3 BMDCs. The alpha myosin, ANP, BNP, and SBK2 peptide library was generated as 20aa peptides with 5aa overlaps from GenScript. Due to insolubility in aqueous solution, two 20aa peptides were replaced by three 10aa peptides each. Sequences of all 172 peptides are shown in Extended Data Table 1. Peptides were added at a concentration of 10μg/mL and co-cultures were incubated overnight. TCR cell lines were stained with DAPI to assess viability and analyzed via flow cytometry for NFAT-GFP reporter activity. For the human TCR (TCR-Pt1), autologous LCLs were used as APCs. TCR-Pt1 was screened against 130 alpha-myosin peptides.

MHC blocking.

Jurkat TCR cell lines were co-cultured with EL-4 cells as APCs with or without 10μg/mL cognate peptide overnight. EL-4 cells were a gift from Dr. Simon Mallal. Blocking antibodies (anti-Db clone 28-14-8S or anti-Kb clone B8-24-3) were added to cells at a concentration of 10μg/mL for 1 hour prior to adding peptides. Blocking antibodies were generously provided by Dr. John Sidney. TCR cell lines were stained with Thy1.1-APC/Cy7 (BioLegend, cat# 202506, Clone OX-7, dilution 1:500) to differentiate from EL-4s and with DAPI to assess viability and analyzed via flow cytometry for NFAT-GFP reporter activity.

Patients.

All studies were conducted in accordance with the Declaration of Helsinki principles under protocols approved by the Vanderbilt University Medical Center (VUMC) Institutional Review Board. Healthy donors provided informed consent under an institutionally approved protocol (IRB# 030062). Myocarditis patients and families provided informed consent for research use of biospecimens and clinical data (IRB# 191213). ICI-colitis and Crohn's patients provided informed consent for research use of biospecimens and clinical data (IRB# 09109). Cardiac transplant and heart failure patients provide informed consent for research use of biospecimens and clinical data (IRB #200551). Patients in RNA-sequencing cohort were previously published[35]. An additional melanoma gene expression dataset was generated by the TCGA Research Network: https://www.cancer.gov/tcga and accessed using cBioPortal[57,58].

Generation of LCLs from PBMC.

EBV-transformed lymphoblastoid B cell lines were generated from cryopreserved donor PBMCs by infection with EBV virus stock[59,60]. Approximately, $1\text{-}3 \times 10^6$ PBMCs in

RPMI-1640 media supplemented with non-heat inactivated 20% fetal bovine serum (FBS), 1 µg/mL cyclosporin A (CSA; Sigma-Aldrich C1832), and 2.5 µg/mL CpG (Invitrogen ODN2006) were infected with filtered EBV stock and cultured for 2-3 weeks, until clusters of cells were visible by light microscopy.

PBMC expansion.

PBMCs were isolated from EDTA collection tubes and processed using a Ficoll gradient. Antigen-specific PBMC expansion was adapted from previously described protocols[61,62]. Fresh or cryopreserved PBMCs were stimulated with 130 pooled alpha-myosin peptides at a final concentration of 400ng/mL of each peptide or a pool of control CMV, EBV, and flu (CEF) peptides (AnaSpec, AS-61036-003). PBMCs were cultured in CTS OpTmizer medium (CTS OpTmizer T Cell Expansion SFM with CTS supplement A1048501, substituted with 2mM L-glutamine, and 2% human serum, Sigma-Aldrich, H3667) with cytokine supplementation (25ng/mL each of rhIL-2, rhIL-7 and rhIL-15, Peprotech). For myocarditis patients 1,2, and 3, expansion cultures were also supplemented with autologous LCLs to serve as antigen presenting cells at a ratio of 1 APC per 10 PBMC. For healthy donors, expansion was done directly from fresh, not cryopreserved, blood. Peptides were only added on the first day of culture. On day 3, additional media with cytokines was added. On day 7, cells were transferred to a new culture dish with fresh media with cytokines. Cells were analyzed or cryopreserved on day 14.

Single cell sequencing of exPBMC.

Expanded PBMCs (exPBMC) from patient 1 were prepared for single cell sequencing as follows. exPBMC were incubated with Human TruStain FcX™ (Fc Receptor Blocking Solution; BioLegend cat# 422302, dilution 1:100) for 5 minutes on ice, then washed and incubated with human anti-CD3-AF488 (BioLegend, cat# 300319, clone HIT3a, dilution 1:200) for 30 minutes on ice, and then washed and resuspended to a concentration of $5x10^5$ cells/mL. SYTOX AADvanced™ Ready Flow™ Reagent (Invitrogen, cat# R37173, dilution 2 drops per 1mL) was used following the manufacturer's instructions to exclude dead cells. CD3+ live cells were sorted on the WOLF cell sorter (Nanocellect). Cells were sequenced and data were analyzed as described above. Data were analyzed in R using the filtered h5 gene matrices in the Seurat package[52-54]. Briefly, samples were subset to include cells with greater than 200 but less than 4000 unique transcripts to exclude likely non-cellular RNA reads and doublets. Cells with greater than 15% of reads coming from mitochondrial transcripts were also excluded as likely dying cells. Clonal is defined as more than two cells with the same TCR clonotype (defined by unique combinations of CDR3 regions). For exPBMC, 5,816 cells with TCR reads were analyzed. To identify TCRs overlapping with the cardiac repertoire, beta CDR3 sequences were used.

Tetramer staining and flow cytometry.

Murine tetramer staining was done using an empty H-2Kb-PE tetramer (Tetramer Shop). Empty tetramer was loaded with peptide by incubating 5µL of empty tetramer with 0.5µL of 200µM peptide solution (all peptides custom ordered from GenScript, in this case VIQYFASI, VQQVYYSI or SIINFEKL as an irrelevant peptide control which is known to bind to H-2Kb strongly) for at least 30 minutes at 4°C. Loaded tetramers were centrifuged

at 3300xg for 5 minutes prior to use. Murine hearts were dissociated as above. Cells were first stained with Zombie Violet (BioLegend, cat # 423113, dilution 1:1000) for 15 minutes at room temperature in PBS with no added protein. Cells were then incubated with TruStain FcX block (BioLegend, cat # 101319, clone 93, dilution 1:100) for 5 minutes at room temperature. Cells were washed in PBS + 2%FBS. Cells were stained with 5μL of loaded tetramer in 50 μL PBS+2% FBS for 20 minutes at 37°C. Without washing 20 μL of solution containing desired surface antibodies was added and cells were incubated for 20 minutes at 4°C. Surface antibodies used were anti-CD3-APC (BioLegend, cat# 100235, clone 17A2, dilution 1:400) and anti-CD8a-FITC (Thermo Fisher, cat # MA5-16759, clone KT15, dilution 1:200). Samples were washed and then analyzed.

Human tetramer staining was done using empty tetramers easYmer HLA-A*03:01 (Eagle Biosciences, cat # 1016-01-20) or easYmer HLA-A*24:02 (Eagle Biosciences, cat # 1020-01-20). Monomers were loaded with peptide following the manufacturer's instructions and incubated for 48 hours at 18°C. Tetramers were produced by adding 2.1 μL of Streptavidin-PE antibody (BioLegend, cat# 405203) and incubating for at least 1 hour at 4°C. Cells were first stained with Zombie Violet (BioLegend, cat # 423113, dilution 1:1000) for 15 minutes at room temperature in PBS with no added protein. Cells were then incubated with TruStain FcX block (BioLegend, cat # 422301, dilution 1:200). Cells were stained with tetramer in PBS with 2% FBS for 20 minutes at room temperature. Cells were then washed and stained with surface antibodies anti-CD3-AF488 (BioLegend, cat# 300319, clone HIT3a, dilution 1:200) and anti-CD8a-APC (BioLegend, Cat # 301014, clone RPA-T8, dilution 1:200) for 20 minutes at 4°C. Samples were washed in PBS with 2% FBS. Samples were run on an Attune NxT Acoustic Focusing Cytometer (Life Technologies). Analysis was performed in FlowJo. Gating was first done on forward scatter and side scatter to exclude debris. Doublets were excluded by gating on FSC area versus FSC height. Zombie Violet was used to exclude dead cells from analyses.

Statistical analysis.

All statistical analyses were performed in R v4.1.1. All single-cell statistical analyses were calculated in R using the Seurat package[52-54]. Visualization and graph generation was performed in R. Shannon diversity was calculated using the R package vegan[63]. The R package immunarch was used for evaluating TCR repertoires[64]. P-value cut-offs displayed on plots correspond to "ns" equals $p>0.05$, * equals $0.01<p<0.05$, ** equals $0.001<p<0.01$, *** equals $0.0001<p<0.001$, **** equals $p<0.0001$.

Extended Data
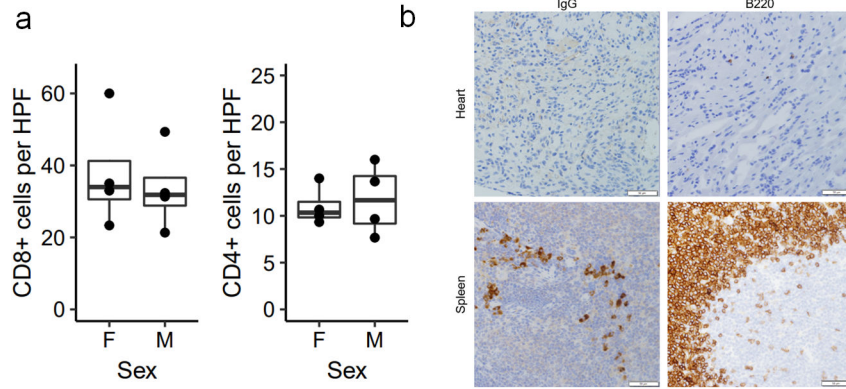
Extended Data Figure 1. Myocardial immune infiltrate does not differ by sex.
a) Quantification of immunohistochemistry (IHC) for CD8 and CD4 in male and female *Pdcd1−/−Ctla4+/−* mice with MC. Cells are counted as number of positive cells per high power (40x) field (HPF). Each data point represents an average of three high power fields per mouse. n=4 female mice, n=4 male mice. Box plots show the median, first and third quartiles. The whiskers extend to the maxima and minima but no further than 1.5 times the inter-quartile range. b) Representative IHC for IgG and B220 (CD45R) in hearts of mice with MC and positive control staining in spleen. Images are representative of n=8 independent *Pdcd1−/−Ctla4+/−* mice with MC (n=4 male; n=4 female). Scale bars represent 50μm.
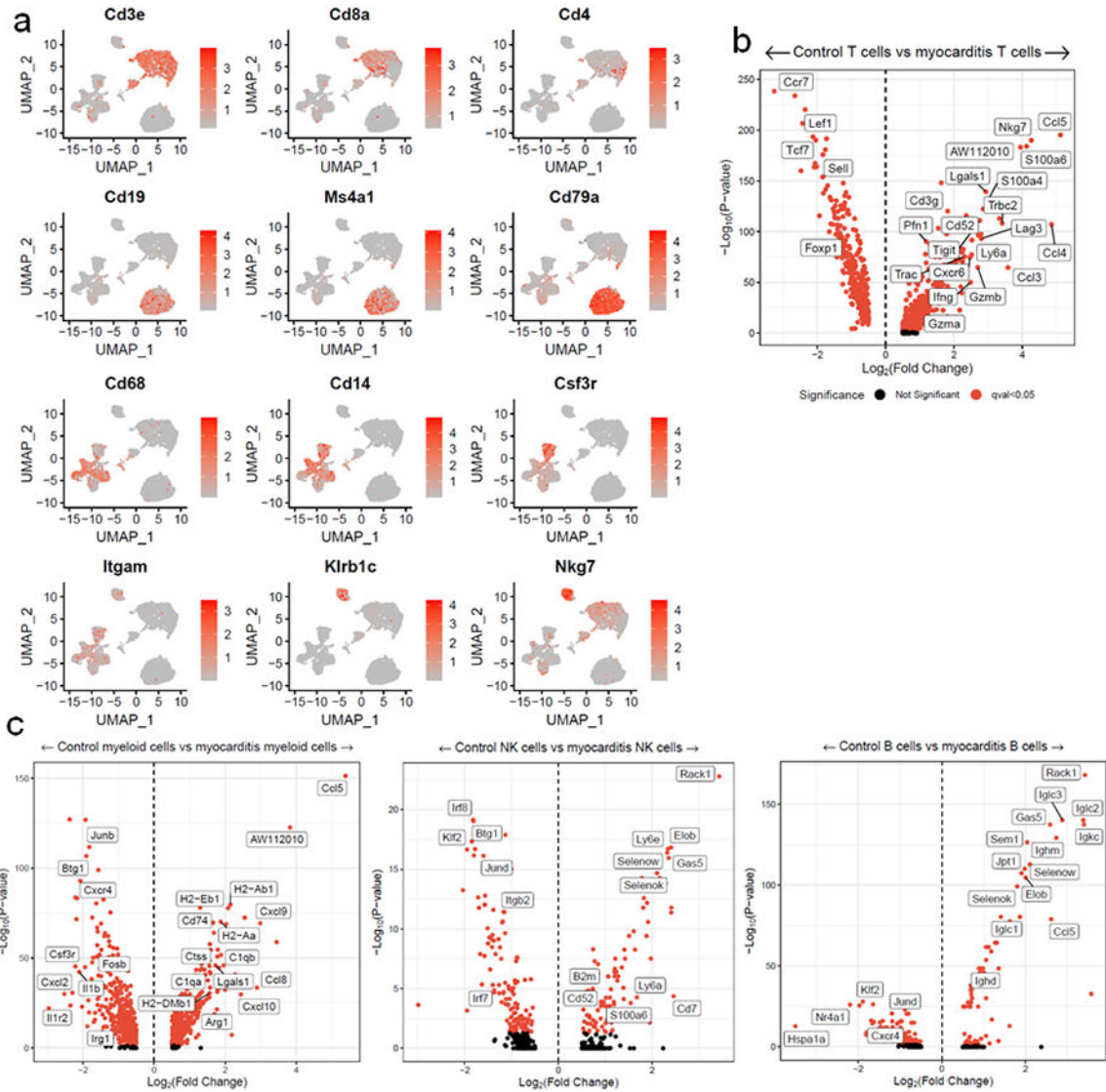
Extended Data Figure 2. MC is characterized by activated immune cells and clonal T cells.
a) Gene expression of key identity genes, showing cell types of clusters. b) Differential gene expression for T, c) myeloid, B and NK cells in MC compared to control cardiac CD45+ cells. Red indicates FDR-corrected p-value (q-value) <0.05. Black indicates not significant.
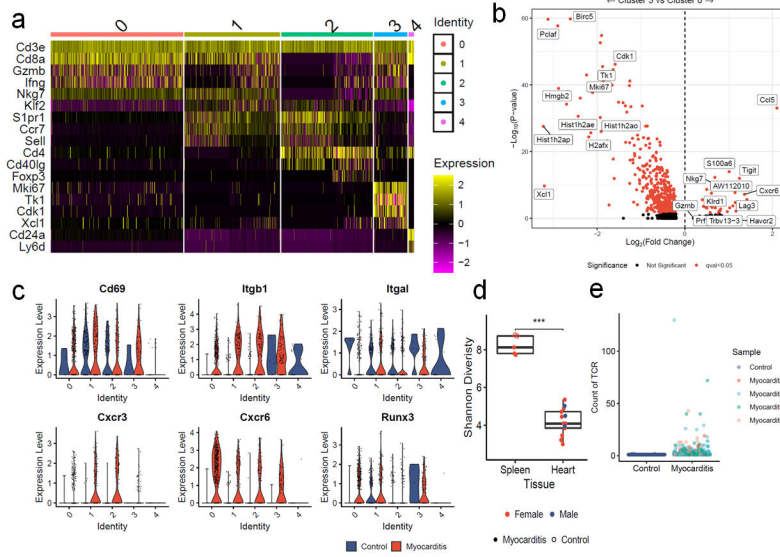
Extended Data Figure 3. T cells in MC are effector or proliferating, tissue-resident and clonal.
a) Expression of key T cell genes by cluster in single cell data. b) Differential gene expression for Cluster 0 vs. Cluster 3 T cells. Red indicates FDR-corrected p-value (q-value) <0.05. Black indicates not significant. c) Violin plots show expression of key tissue residency associated genes by cluster and MC vs. control. d) Shannon diversity on bulk TCR sequencing beta chain repertoires. Color indicates sex. Shape indicates whether the tissue was derived from a control wild type mouse (open circle) or a *Pdcd1−/−Ctla4+/−* mouse with MC (filled circle). P=0.0002, two-sided Wilcoxon test. Box plots show the median, first and third quartiles. The whiskers extend to the maxima and minima but no further than 1.5 times the inter-quartile range. e) TCR counts in single cell data. MC sample is divided by mouse of origin. Clonal TCRs are found in all 4 sequenced hearts.
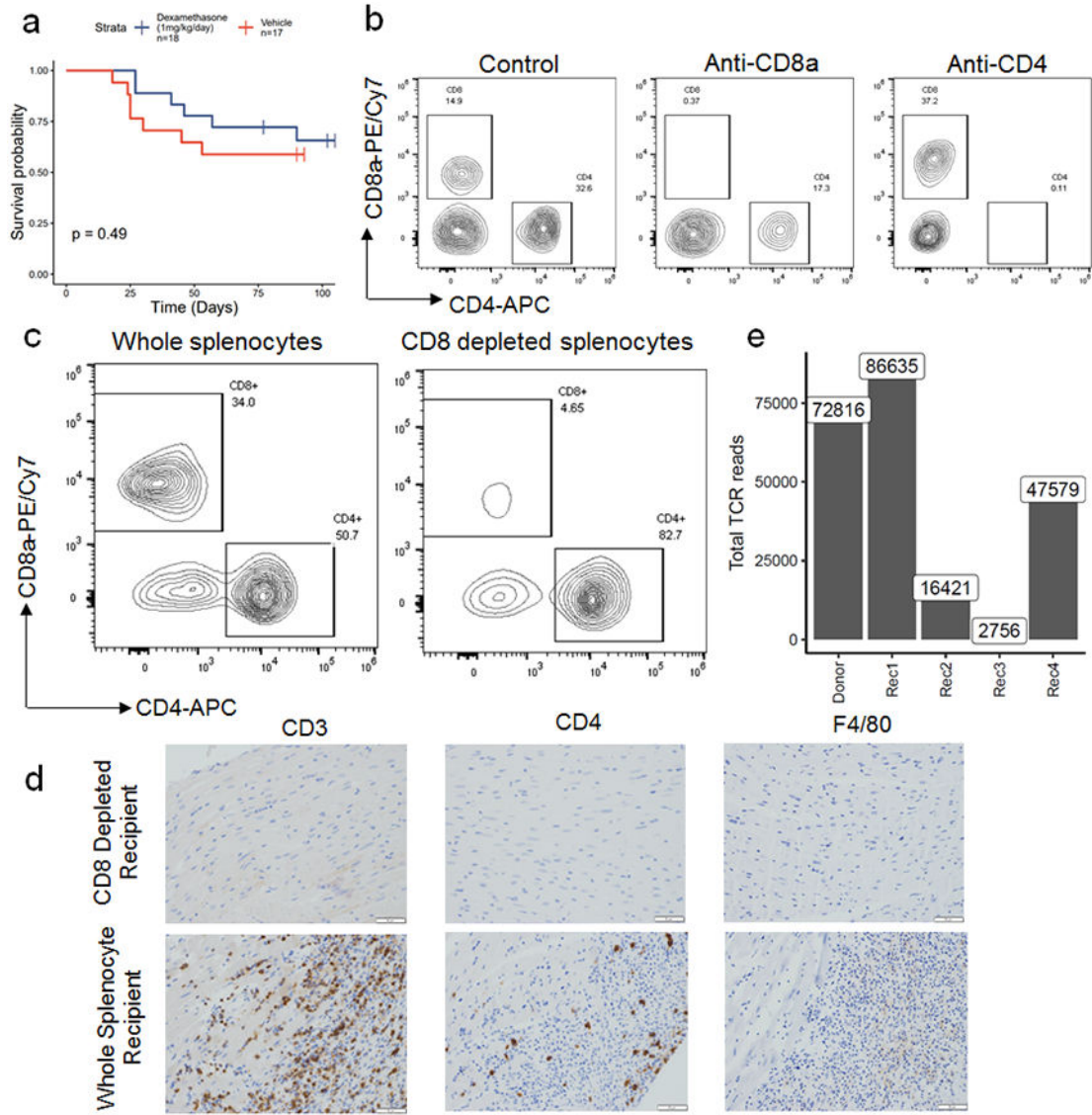
Extended Data Figure 4. Confirmation of cell type depletion.
a) Female *Pdcd1−/−Ctla4+/−* mice were treated with dexamethasone (1mg/kg/day; n=18) or vehicle (n=17) starting at 21 days of life. Time is measured since birth. P=0.49, two-sided cox proportional hazard test. b) Representative flow cytometry gated on live CD45+ cells isolated from blood of different treatment groups, at week 3 of treatment. c) Representative flow cytometry on CD8 depleted (via magnetic beads) compared to whole splenocytes used for adoptive transfer. d) Representative immunohistochemistry on hearts of a CD8 depleted splenocyte recipient compared to a whole splenocyte recipient. Only cardiac sections are shown. Scale bars show 50μm. Representative of n=10 animals per group. e) Total TCR reads for cardiac TCR beta chain sequencing on donor and recipient hearts.
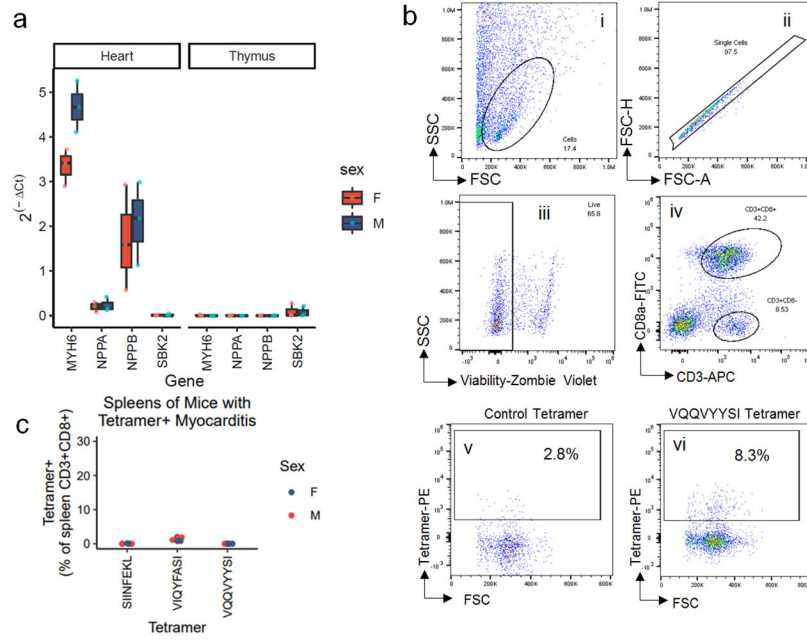
Extended Data Figure 5. Thymic expression of Myh6 and flow cytometry gating for murine α-myosin tetramers.

a) Gene expression for *Myh6, Nppa, Nppb,* and *Sbk2* in the heart and thymus of n=3 each male and female *Pdcd1−/−Ctla4+/−* mice. Gene expression is normalized to beta-actin. Gene expression is plotted as 2^-(Ct gene of interest minus Ct of beta-actin). Box plots show the median, first and third quartiles. The whiskers extend to the maxima and minima but no further than 1.5 times the inter-quartile range. b) Gating strategy for H2-Kb tetramers on murine heart samples. Debris, doublets and dead cells (Zombie Violet positive) are excluded. CD3+CD8+ cells are used for tetramer analysis. Staining for Control (SIINFEKL) H2-Kb, and VQQVYYSI H2-Kb tetramers are shown. c) Quantification of spleen tetramer positive CD3+CD8+ cells, by sex of the mouse. The spleens used in this experiment correspond to the mice show in Fig. 3f, which all have α-myosin tetramer positive MC.
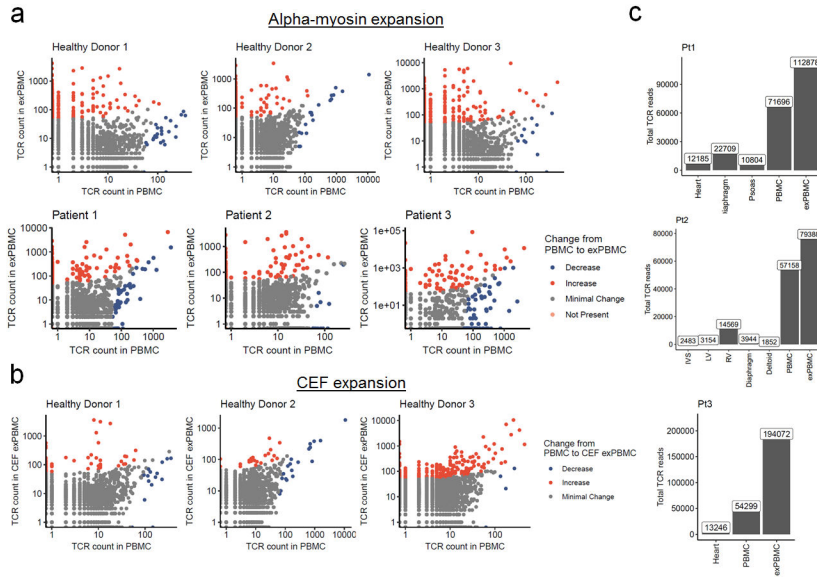
Extended Data Figure 6. TCR sequencing on exPBMC shows expansion of α-myosin and CEF specific TCRs.

a) Comparison of TCR beta chain abundance in α-myosin exPBMC and pre-expansion PBMC for all patients. Each plot is within the same patient only. Color represents change from PBMC to exPBMC. Minimal change is less than a 50 read count change. b) Comparison of TCR beta chain abundance in CEF exPBMC and pre-expansion PBMC for all healthy donors. Color represents change from PBMC to CEF exPBMC. Minimal change is less than a 50 read count change. c) Total TCR reads for biopsy (heart), autopsy, and PBMC samples from patients 1, 2 and 3.
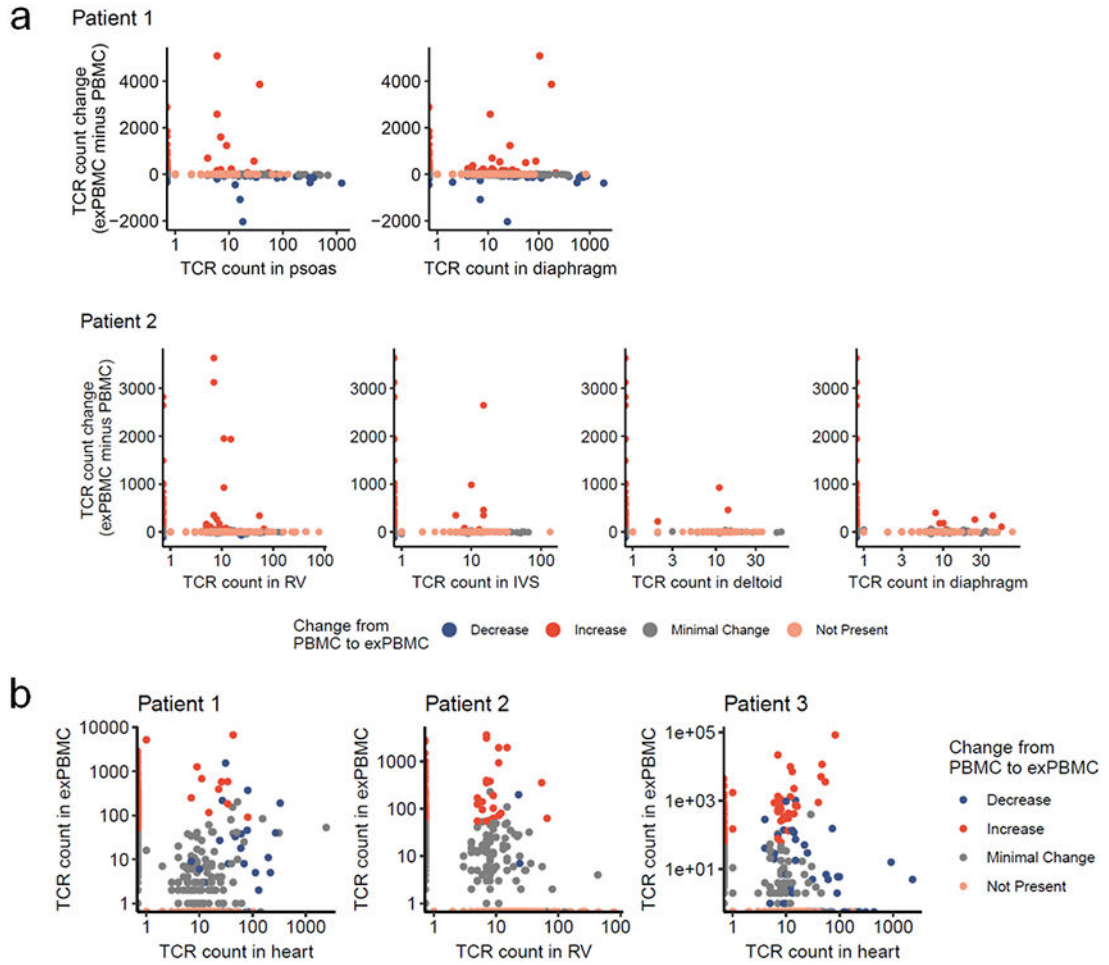
Extended Data Figure 7. α-myosin expanded TCRs are found in the hearts and skeletal muscles of patients with ICI-MC.

a) Change in TCR counts from PBMC to α-myosin exPBMC plotted by abundance of the same TCR beta chain in the autologous inflamed cardiac or skeletal muscle tissue of each patient. Minimal change is less than a 50 read count change. Not present means not found in either PBMC or exPBMC, but present in indicated tissue. b) Comparison of TCR beta chain abundance in α-myosin exPBMC and heart (biopsy for patient 1 and 3 or right ventricle for patient 2). Color represents change from PBMC to exPBMC. Minimal change is less than a 50 read count change. Not present means not found in either PBMC or exPBMC, but present in heart.
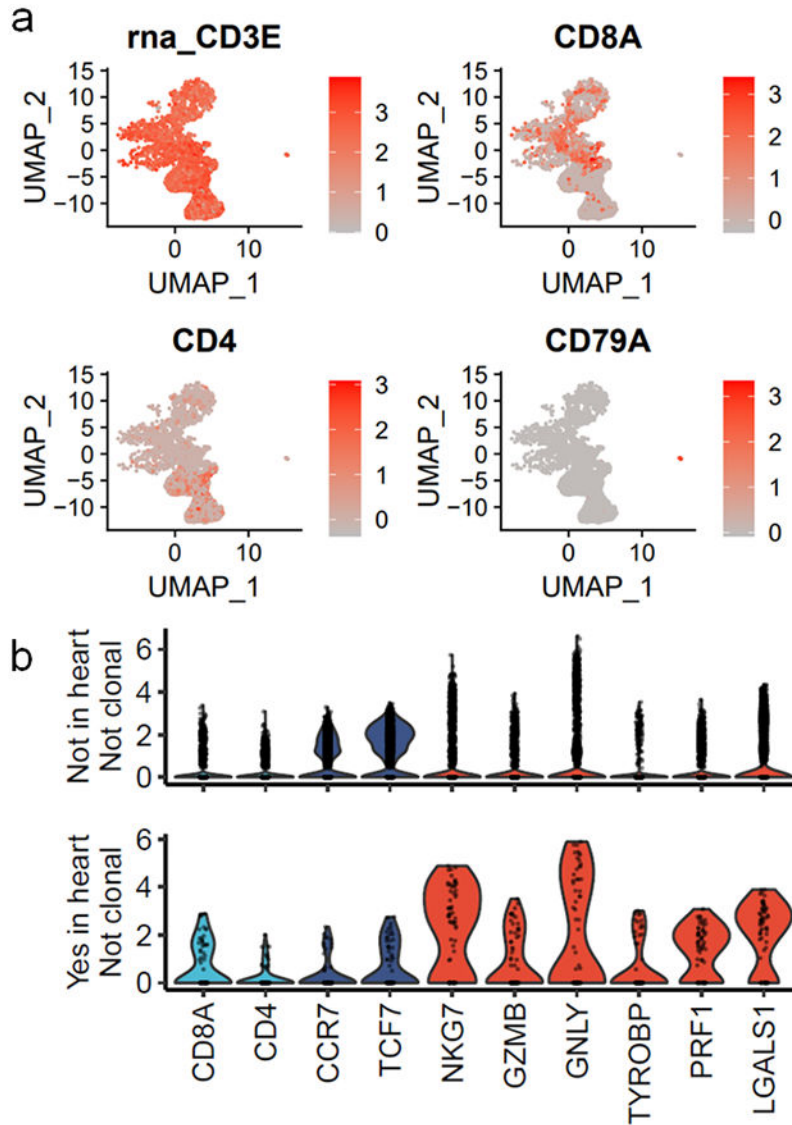
Extended Data Figure 8. Purity analysis for single cell sequencing on exPBMCs from patient 1.
a) Gene expression is shown on single cell sequencing of CD3 sorted exPBMCs from patient 1. b) Violin plots of key gene expression by presence or absence in cardiac TCR repertoire and clonality in exPBMC. Identity genes are shown in light blue. Genes associated with naïve T cells are shown in dark blue. Genes associated with T cell activation are shown in red.
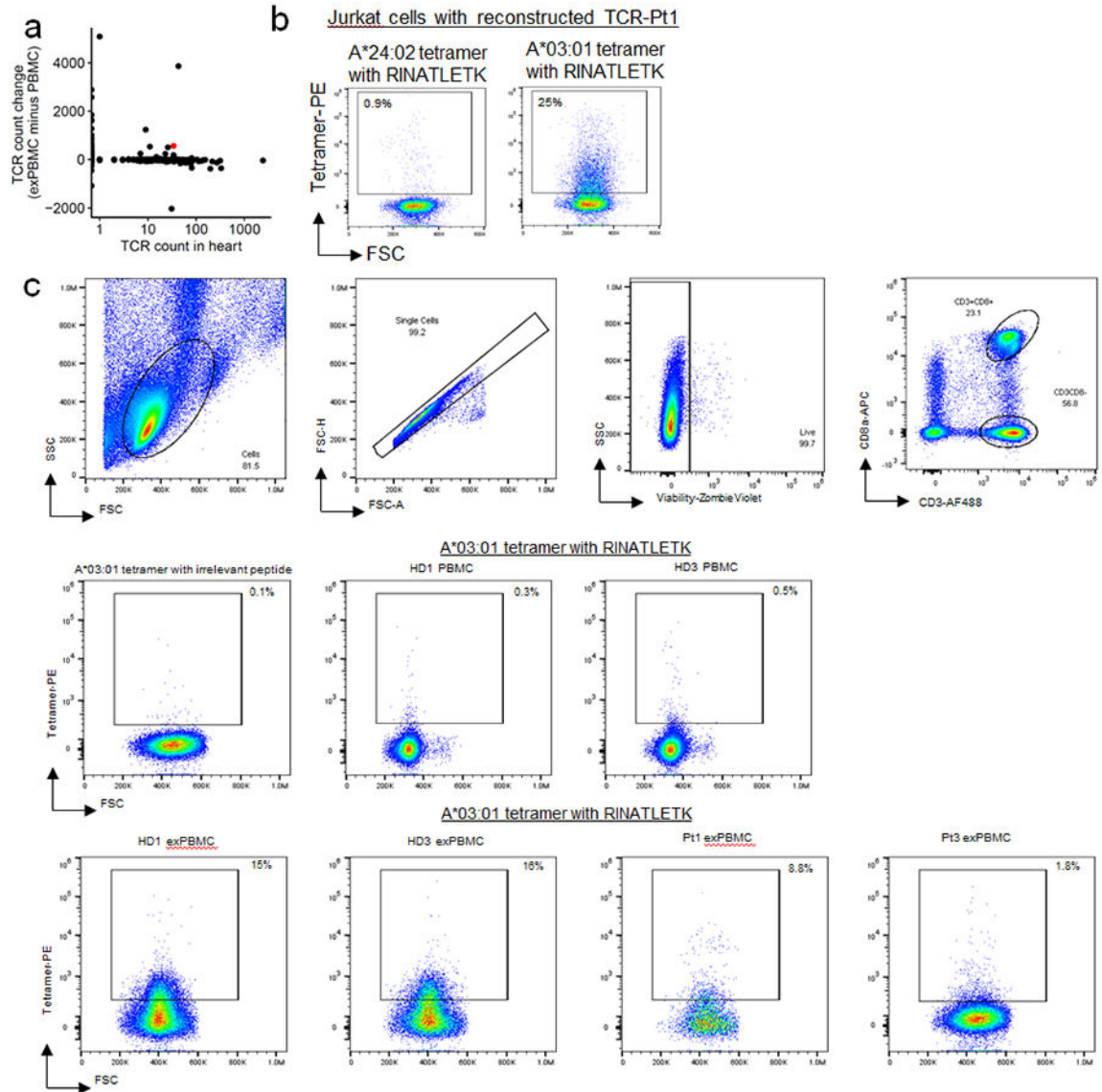
Extended Data Figure 9. TCR from Pt 1 exPBMC recognizes α-myosin epitope.
a) TCR-Pt1, which was cloned and transduced into Jurkat NFAT-GFP reporter cells, is shown in red on the same plot show in Fig 4c. This shows the expansion of this TCR in the exPBMC and abundance in the heart. b) Representative flow cytometry scatter plots are shown for the TCR-pt1 Jurkat cell line is stained with A*24:02 tetramer with RINATLETK or A*03:01 tetramer with RINATLETK. c) Full flow cytometry gating strategy for human PBMC and exPBMC tetramer staining. Debris, doublets and dead cells (Zombie Violet positive) are excluded. CD3+CD8+ cells are used for tetramer analysis. Tetramer staining for all samples is shown.
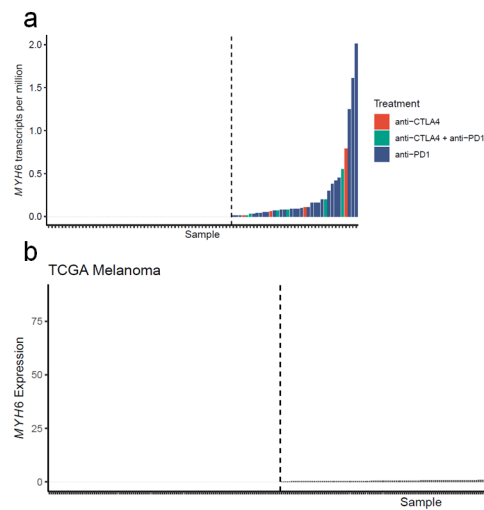
Extended Data Figure 10. Tumor-specific MYH6 expression.

a) *MYH6* transcripts per million are shown for n=91 pre-treatment RNA-sequencing melanoma samples. Bars are colored by what ICI treatment the patient received. b) *MYH6* expression is shown for n=363 melanoma samples accessed from TCGA. Samples to the right of the dotted lines have detectable *MYH6* expression.

Extended Data Table 1.

Amino acid sequences for α-myosin, ANP, BNP and SBK2 peptides included in peptide library.

Name	Sequence	Protein
peptide_1	MTDAQMADFGAAAQYLRKSE	Alpha-myosin
peptide_2	LRKSEKERLEAQTRPFDIRT	Alpha-myosin
peptide_3	FDIRTECFVPDDKEEYVKAK	Alpha-myosin
peptide_4	YVKAKWSREGGKVTAETEN	Alpha-myosin
peptide_5	AETENGKTVTIKEDQVMQQN	Alpha-myosin
peptide_6	VMQQNPPKFDKIEDMAMLTF	Alpha-myosin
peptide_7	AMLTFLHEPAVLYNLKERYA	Alpha-myosin
peptide_9	FCVTVNPYKWLPVYNAEWA	Alpha-myosin
peptide_10	AEWAAYRGKKRSEAPPHIF	Alpha-myosin
peptide_11	PPHIFSISDNAYQYMLTDRE	Alpha-myosin
peptide_12	LTDRENQSILITGESGAGKT	Alpha-myosin
peptide_13	GAGKTVNTKRVIQYFASIAA	Alpha-myosin
peptide_14	ASIAAIGDRSKKENPNANKG	Alpha-myosin
peptide_15	NANKGTLEDQIIQANPALEA	Alpha-myosin
peptide_16	PALEAFGNAKTVRNDNSSRF	Alpha-myosin
peptide_17	NSSRFGKFIRIHFGATGKLA	Alpha-myosin
peptide_18	TGKLASADIETYLLEKSRVI	Alpha-myosin
peptide_20	IFYQILSNKKPELLDMLLVT	Alpha-myosin

Name	Sequence	Protein
peptide_21	MLLVTNNPYDYAFVSQGEVS	Alpha-myosin
peptide_23	LATDSAFDVLSFTAEEKAGV	Alpha-myosin
peptide_24	EKAGVYKLTGAIMHYGNMKF	Alpha-myosin
peptide_25	GNMKFKQKQREEQAEPDGTE	Alpha-myosin
peptide_26	PDGTEDADKSAYLMGLNSAD	Alpha-myosin
peptide_27	LNSADLLKGLCHPRVKVGNE	Alpha-myosin
peptide_28	KVGNEYVTKGQSVQQVYYSI	Alpha-myosin
peptide_29	VYYSIGALAKSVYEKMFNWM	Alpha-myosin
peptide_30	MFNWMVTRINATLETKQPRQ	Alpha-myosin
peptide_31	KQPRQYFIGVLDIAGFEIFD	Alpha-myosin
peptide_32	FEIFDFNSFEQLCINFTNEK	Alpha-myosin
peptide_33	FTNEKLQQFFNHHMFVLEQE	Alpha-myosin
peptide_34	VLEQEEYKKEGIEWEFIDFG	Alpha-myosin
peptide_35	FIDFGMDLQACIDLIEKPMG	Alpha-myosin
peptide_36	EKPMGIMSILEEECMFPKAS	Alpha-myosin
peptide_37	FPKASDMTFKAKLYDNHLGK	Alpha-myosin
peptide_38	NHLGKSNNFQKPRNVKGKQE	Alpha-myosin
peptide_39	KGKQEAHFSLVHYAGTVDYN	Alpha-myosin
peptide_40	TVDYNIMGWLEKNKDPLNET	Alpha-myosin
peptide_41	PLNETWGLYQKSSLKLMAT	Alpha-myosin
peptide_42	KLMATLFSTYASADTGDSGK	Alpha-myosin
peptide_43	GDSGKGKGGKKKGSSFQTVS	Alpha-myosin
peptide_44	FQTVSALHRENLNKLMTNLK	Alpha-myosin
peptide_45	MTNLKTTHPHFVRCIIPNER	Alpha-myosin
peptide_46	IPNERKAPGVMDNPLVMHQL	Alpha-myosin
peptide_47	VMHQLRCNGVLEGIRICRKG	Alpha-myosin
peptide_48	ICRKGFPNRILYGDFRQRYR	Alpha-myosin
peptide_49	RQRYRILNPAAIPEGQFIDS	Alpha-myosin
peptide_50	QFIDSRKGAEKLLGSLDIDH	Alpha-myosin
peptide_51	LDIDHNQYKFGHTKVFFKAG	Alpha-myosin
peptide_52	FFKAGLLGLLEEMRDERLSR	Alpha-myosin
peptide_53	ERLSRIITRIQAQARGQLMR	Alpha-myosin
peptide_54	GQLMRIEFKKIVERRDALLV	Alpha-myosin
peptide_56	VKNWPWMKLYFKIKPLLKSA	Alpha-myosin
peptide_57	LLKSAETEKEMANMKEEFGR	Alpha-myosin
peptide_58	EEFGRVKDALEKSEARRKEL	Alpha-myosin
peptide_59	RRKELEEKMVSLLQEKNDLQ	Alpha-myosin
peptide_60	KNDLQLQVQAEQDNLNDAEE	Alpha-myosin
peptide_61	NDAEERCDQLIKNKIQLEAK	Alpha-myosin

Name	Sequence	Protein
peptide_62	QLEAKVKEMTERLEDEEEMN	Alpha-myosin
peptide_63	EEEMNAELTAKKRKLEDECS	Alpha-myosin
peptide_64	EDECSELKKDIDDLELTLAK	Alpha-myosin
peptide_65	LTLAKVEKEKHATENKVKNL	Alpha-myosin
peptide_66	KVKNLTEEMAGLDEIIAKLT	Alpha-myosin
peptide_67	IAKLTKEKKALQEAHQQALD	Alpha-myosin
peptide_68	QQALDDLQAEEDKVNTLTKS	Alpha-myosin
peptide_69	TLTKSKVKLEQQVDDLEGSL	Alpha-myosin
peptide_70	LEGSLEQEKKVRMDLERAKR	Alpha-myosin
peptide_71	ERAKRKLEGDLKLTQESIMD	Alpha-myosin
peptide_72	ESIMDLENDKLQLEEKLKKK	Alpha-myosin
peptide_73	KLKKKEFDISQQNSKIEDEQ	Alpha-myosin
peptide_74	IEDEQALALQLQKKLKENQA	Alpha-myosin
peptide_75	KENQARIEELEEELEAERTA	Alpha-myosin
peptide_76	AERTARAKVEKLRSDLSREL	Alpha-myosin
peptide_77	LSRELEEISERLEEAGGATS	Alpha-myosin
peptide_78	GGATSVQIEMNKKREAEFQK	Alpha-myosin
peptide_79	AEFQKMRRDLEEATLQHEAT	Alpha-myosin
peptide_80	QHEATAAALRKKHADSVAEL	Alpha-myosin
peptide_81	SVAELGEQIDNLQRVKQKLE	Alpha-myosin
peptide_82	KQKLEKEKSEFKLELDDVTS	Alpha-myosin
peptide_83	DDVTSNMEQIIKAKANLEKV	Alpha-myosin
peptide_84	NLEKVSRTLEDQANEYRVKL	Alpha-myosin
peptide_85	YRVKLEEAQRSLNDFTTQRA	Alpha-myosin
peptide_86	TTQRAKLQTENGELARQLEE	Alpha-myosin
peptide_87	RQLEEKEALISQLTRGKLSY	Alpha-myosin
peptide_88	GKLSYTQQMEDLKRQLEEEG	Alpha-myosin
peptide_89	LEEEGKAKNALAHALQSSRH	Alpha-myosin
peptide_90	QSSRHDCDLLREQYEEEMEA	Alpha-myosin
peptide_91	EEMEAKAELQRVLSKANSEV	Alpha-myosin
peptide_92	ANSEVAQWRTKYETDAIQRT	Alpha-myosin
peptide_93	AIQRTEELEEAKKKLAQRLQ	Alpha-myosin
peptide_94	AQRLQDAEEAVEAVNAKCSS	Alpha-myosin
peptide_95	AKCSSLEKTKHRLQNEIEDL	Alpha-myosin
peptide_96	EIEDLMVDVERSNAAAAALD	Alpha-myosin
peptide_97	AAALDKKQRNFDKILAEWKQ	Alpha-myosin
peptide_98	AEWKQKYEESQSELESSQKE	Alpha-myosin
peptide_99	SSQKEARSLSTELFKLKNAY	Alpha-myosin
peptide_100	LKNAYEESLEHLETFKRENK	Alpha-myosin

Name	Sequence	Protein
peptide_101	KRENKNLQEEISDLTEQLGE	Alpha-myosin
peptide_102	EQLGEGGKNVHELEKIRKQL	Alpha-myosin
peptide_103	IRKQLEVEKLELQSALEEAE	Alpha-myosin
peptide_104	LEEAEASLEHEEGKILRAQL	Alpha-myosin
peptide_105	LRAQLEFNQIKAEIERKLAE	Alpha-myosin
peptide_106	RKLAEKDEEMEQAKRNHLRM	Alpha-myosin
peptide_108	ETRSRNEALRVKKKMEGDLN	Alpha-myosin
peptide_109	EGDLNEMEIQLSQANRIASE	Alpha-myosin
peptide_110	RIASEAQKHLKNSQAHLKDT	Alpha-myosin
peptide_111	HLKDTQLQLDDAVHANDDLK	Alpha-myosin
peptide_112	NDDLKENIAIVERRNNLLQA	Alpha-myosin
peptide_113	NLLQAELEELRAWEQTERS	Alpha-myosin
peptide_114	QTERSRKLAEQELIETSERV	Alpha-myosin
peptide_115	TSERVQLLHSQNTSLINQKK	Alpha-myosin
peptide_116	INQKKKMESDLTQLQTEVEE	Alpha-myosin
peptide_117	TEVEEAVQECRNAEEKAKKA	Alpha-myosin
peptide_118	KAKKAITDAAMMAEELKKEQ	Alpha-myosin
peptide_119	LKKEQDTSAHLERMKKNMEQ	Alpha-myosin
peptide_120	KNMEQTIKDLQHRLDEAEQI	Alpha-myosin
peptide_121	EAEQIALKGGKKQLQKLEAR	Alpha-myosin
peptide_122	KLEARVRELENELEAEQKRN	Alpha-myosin
peptide_123	EQKRNAESVKGMRKSERRIK	Alpha-myosin
peptide_124	ERRIKELTYQTEEDKKNLMR	Alpha-myosin
peptide_125	KNLMRLQDLVDKLQLKVKAY	Alpha-myosin
peptide_126	KVKAYKRQAEEAEEQANTNL	Alpha-myosin
peptide_127	ANTNLSKFRKVQHELDEAEE	Alpha-myosin
peptide_128	DEAEERADIAESQVNKLRAK	Alpha-myosin
peptide_129	KLRAKSRDIGAKKMHDEE	Alpha-myosin
19A	KSRVIFQLKA	Alpha-myosin
19B	FQLKAERNYH	Alpha-myosin
19C	ERNYHIFYQI	Alpha-myosin
55A	DALLVIQWNI	Alpha-myosin
55B	IQWNIRAFMG	Alpha-myosin
55C	RAFMGVKNWP	Alpha-myosin
SBK2_1	MPGKQSEDKPMEVSTVEDGG	SBK2
SBK2_2	VEDGGDEGLGGLTVEELQQG	SBK2
SBK2_3	ELQQGQEAALALEDMMALSA	SBK2
SBK2_4	MALSAQTLVQTEVEELYEEV	SBK2
SBK2_5	LYEEVRPLGQGRFGRVLLVT	SBK2

Name	Sequence	Protein
SBK2_6	VLLVTHRQKGTPLALKQLPK	SBK2
SBK2_7	KQLPKQSTSLRGFLYEFCVG	SBK2
SBK2_8	EFCVGLSLGTH SAIVTAYG1	SBK2
SBK2_9	TAYGIGIESANSYSFLTEPV	SBK2
SBK2_10	LTEPVLHGDLITFIQPKVGL	SBK2
SBK2_11	PKVGLPQPAAQRCAAQLASA	SBK2
SBK2_12	QLASALEHIHSHGLVYRDLK	SBK2
SBK2_13	YRDLKPENVLVCDPACQRVK	SBK2
SBK2_14	CQRVKLTDFGHTRPRGTLLR	SBK2
SBK2_15	GTLLRLTGPPIPYTAPELCA	SBK2
SBK2_16	PELCAPPPLPEGLPIQPSLD	SBK2
SBK2_17	QPSLDAWALGVLIFCLLTGY	SBK2
SBK2_18	LLTGYFPWDQPLVEVDPFFE	SBK2
SBK2_19	DPFFEDFLIWQASGQPQDRP	SBK2
SBK2_20	PQDRPQPWYSLSPAADTLLW	SBK2
SBK2_21	DTLLWGLLDPHPRKRNPVGS	SBK2
SBK2_22	NPVGSIKSYLGQPWKQREGE	SBK2
SBK2_23	QREGEAEELATELREDGWRG	SBK2
SBK2_24	DGWRGGQEAAKGEQPAC	SBK2
NPPA_26	FWLPGHIGANPVYSAVSNTD	ANP
NPPA_27	VSNTDLMDFKNLLDHLEEKM	ANP
NPPA_28	LEEKMPVEDEVMPPQALSEQ	ANP
NPPA_29	ALSEQTEEAGAALSSLPEVP	ANP
NPPA_30	LPEVPPWTGEVNPPLRDGSA	ANP
NPPA_31	RDGSALGRSPWDPSDRSALL	ANP
NPPA_32	RSALLKSKLRALLAGPRSLR	ANP
NPPA_33	PRSLRRSSCFGGRIDRIGAQ	ANP
NPPA_34	RIGAQSGLGCNSFRYRR	ANP
BNP_35	MDLLKVLSQMILFLLFLYLS	BNP
BNP_36	FLYLSPLGGHSYPLGSPSQS	BNP
BNP_37	SPSQSPEQFKMQKLLELIRE	BNP
BNP_38	ELIREKSEEMAQRQLLKDQG	BNP
BNP_39	LKDQGLTKEHPKRVLRSQGS	BNP
BNP_40	RSQGSTLRVQQRPQNSKVTH	BNP
BNP_41	SKVTHISSCFGHKIDRIGSV	BNP
BNP_42	RIGSVSRLGCNALKLL	BNP

Extended Data Table 2.

Prediction scores for binding of α-myosin peptides to MHC-I molecules in C57BL/6 mice generated by TepiTool.

Seq#	Peptide start	Peptide end	Peptide	Percentile rank	Allele
1	190	198	RVIQYFASI	0.01	H-2-Kb
1	113	120	MIYTYSGL	0.01	H-2-Kb
1	650	660	SALHRENLNKL	0.02	H-2-Db
1	644	652	SSFQTVSAL	0.03	H-2-Kb
1	613	621	SSLKLMATL	0.04	H-2-Db
1	282	290	RNYHIFYQI	0.04	H-2-Kb
1	191	198	VIQYFASI	0.04	H-2-Kb
1	764	771	KVFFKAGL	0.05	H-2-Kb
1	824	832	MGVKNWPWM	0.06	H-2-Db
1	322	330	ASIDDSEEL	0.06	H-2-Db
1	827	834	KNWPWMKL	0.06	H-2-Kb
1	613	621	SSLKLMATL	0.06	H-2-Kb
1	1759	1767	KAITDAAMM	0.07	H-2-Db
1	644	652	SSFQTVSAL	0.07	H-2-Db
1	1242	1250	KAKANLEKV	0.07	H-2-Db
1	730	738	AAIPEGQFI	0.08	H-2-Db
1	684	692	GVMDNPLVM	0.08	H-2-Db
1	479	486	INFTNEKL	0.08	H-2-Kb
1	909	917	QUKNKIQL	0.09	H-2-Db
1	1893	1901	TNLSKFRKV	0.11	H-2-Kb
1	421	428	VYYSIGAL	0.12	H-2-Kb
1	356	363	AIMHYGNM	0.12	H-2-Kb
1	148	157	SEAPPHIFSI	0.13	H-2-Db
1	1890	1898	QANTNLSKF	0.13	H-2-Db
1	155	165	FSISDNAYQYM	0.14	H-2-Db
1	279	287	KAERNYHIF	0.14	H-2-Db
1	311	319	YAFVSQGEV	0.14	H-2-Db
1	487	495	QQFFNHHMF	0.16	H-2-Db
1	149	157	EAPPHIFSI	0.17	H-2-Db
1	113	121	MIYTYSGLF	0.17	H-2-Kb
1	243	251	SRFGKFIRI	0.18	H-2-Kb
1	649	657	VSALHRENL	0.18	H-2-Kb
1	282	291	RNYHIFYQIL	0.18	H-2-Kb
1	724	732	YRILNPAAI	0.19	H-2-Db
1	487	497	QQFFNHHMFVL	0.2	H-2-Db
1	335	342	SAFDVLSF	0.2	H-2-Kb

Seq#	Peptide start	Peptide end	Peptide	Percentile rank	Allele
1	765	772	VFFKAGLL	0.2	H-2-Kb
1	147	157	RSEAPPHIFSI	0.21	H-2-Db
1	1520	1528	EGGKNVHEL	0.21	H-2-Db
1	666	674	TTHPHFVRC	0.21	H-2-Kb
1	431	439	SVYEKMFNW	0.21	H-2-Kb
1	650	657	SALHRENL	0.21	H-2-Kb
1	1587	1595	QAKRNHLRM	0.22	H-2-Db
1	682	692	APGVMDNPLVM	0.22	H-2-Db
1	1563	1570	AQLEFNQI	0.22	H-2-Kb
1	418	425	VQQVYYSI	0.22	H-2-Kb
1	1674	1682	AIVERRNNL	0.23	H-2-Kb
1	881	891	SLLQEKNDLQL	0.24	H-2-Db
1	681	690	KAPGVMDNPL	0.24	H-2-Db
1	260	268	ASADIETYL	0.25	H-2-Db
1	1791	1799	TIKDLQHRL	0.25	H-2-Kb
1	454	461	RQYFIGVL	0.25	H-2-Kb
1	1490	1500	YEESLEHLETF	0.26	H-2-Db
1	284	291	YHIFYQIL	0.26	H-2-Kb
1	764	772	KVFFKAGLL	0.26	H-2-Kb
1	420	428	QVYYSIGAL	0.26	H-2-Kb
1	834	841	LYFKIKPL	0.29	H-2-Kb
1	355	363	GAIMHYGNM	0.29	H-2-Kb
1	76	84	VMQQNPPKF	0.3	H-2-Db
1	487	494	QQFFNHHM	0.3	H-2-Kb
1	125	133	VNPYKWLPV	0.3	H-2-Kb
1	1291	1299	RQLEEKEAL	0.31	H-2-Db
1	657	664	LNKLMTNL	0.31	H-2-Kb
1	320	330	SVASIDDSEEL	0.32	H-2-Db
1	1207	1215	EQIDNLQRV	0.32	H-2-Db
1	834	842	LYFKIKPLL	0.32	H-2-Kb
1	271	278	KSRVIFQL	0.32	H-2-Kb
1	545	553	SDMTFKAKL	0.32	H-2-Kb
1	1492	1500	ESLEHLETF	0.33	H-2-Db
1	384	391	KSAYLMG	0.33	H-2-Kb
1	437	444	FNWMVTRI	0.35	H-2-Kb
1	1861	1869	KNLMRLQDL	0.35	H-2-Kb
1	1257	1265	QANEYRVKL	0.35	H-2-Kb
1	157	165	ISDNAYQYM	0.37	H-2-Kb
1	417	425	SVQQVYYSI	0.37	H-2-Kb

Seq#	Peptide start	Peptide end	Peptide	Percentile rank	Allele
1	490	497	FNHHMFVL	0.37	H-2-Kb
1	833	841	KLYFKIKPL	0.39	H-2-Kb
1	123	131	VTVNPYKWL	0.39	H-2-Kb
1	441	448	VTRINATL	0.39	H-2-Kb
1	883	891	LQEKNDLQL	0.4	H-2-Db
1	1409	1416	VNAKCSSL	0.41	H-2-Kb
1	261	269	SADIETYLL	0.42	H-2-Db
1	1484	1494	FKLKNAYEESL	0.42	H-2-Kb
1	322	331	ASIDDSEELL	0.43	H-2-Db
1	1239	1247	QIIKAKANL	0.43	H-2-Kb
1	79	87	QNPPKFDKI	0.43	H-2-Kb
1	649	657	VSALHRENL	0.44	H-2-Db
1	607	615	VGLYQKSSL	0.44	H-2-Kb
1	467	474	EIFDFNSF	0.44	H-2-Kb
1	431	440	SVYEKMFNWM	0.44	H-2-Kb
1	562	570	NNFQKPRNV	0.44	H-2-Db
1	355	363	GAIMHYGNM	0.45	H-2-Db
1	288	298	YQILSNKKPEL	0.45	H-2-Db
1	487	496	QQFFNHHMFV	0.46	H-2-Db
1	93	101	LTFLHEPAV	0.46	H-2-Kb
1	823	832	FMGVKNWPWM	0.47	H-2-Db
1	1655	1663	TQLQLDDAV	0.47	H-2-Db
1	242	251	SSRFGKFIRI	0.47	H-2-Kb
1	1258	1265	ANEYRVKL	0.48	H-2-Kb
1	1240	1247	IIKAKANL	0.48	H-2-Kb
1	920	928	KVKEMTERL	0.49	H-2-Kb
1	1479	1486	LSTELFKL	0.5	H-2-Kb
1	614	621	SLKLMATL	0.5	H-2-Kb
1	592	602	MGWLEKNKDPL	0.51	H-2-Db
1	971	980	HATENKVKNL	0.51	H-2-Db
1	1783	1792	RMKKNMEQTI	0.51	H-2-Db
1	388	396	LMGLNSADL	0.52	H-2-Db
1	229	237	EAFGNAKTV	0.52	H-2-Db
1	594	602	WLEKNKDPL	0.52	H-2-Db
1	149	157	EAPPHIFSI	0.52	H-2-Kb
1	1831	1839	EQKRNAESV	0.53	H-2-Db
1	156	165	SISDNAYQYM	0.53	H-2-Db
1	389	397	MGLNSADLL	0.53	H-2-Db
1	227	237	ALEAFGNAKTV	0.53	H-2-Kb

Seq#	Peptide start	Peptide end	Peptide	Percentile rank	Allele
1	164	174	YMLTDRENQSI	0.54	H-2-Db
1	1223	1230	KSEFKLEL	0.54	H-2-Kb
1	321	330	VASIDDSEEL	0.56	H-2-Db
1	1544	1553	SALEEAEASL	0.56	H-2-Db
1	311	321	YAFVSQGEVSV	0.57	H-2-Db
1	487	495	QQFFNHHMF	0.57	H-2-Kb
1	251	259	IHFGATGKL	0.57	H-2-Kb
1	816	824	IQWNIRAFM	0.59	H-2-Kb
1	488	496	QFFNHHMFV	0.59	H-2-Kb
1	999	1009	KALQEAHQQAL	0.6	H-2-Db
1	816	824	IQWNIRAFM	0.6	H-2-Db
1	1109	1117	KLKENQARI	0.6	H-2-Db
1	709	716	KGFPNRIL	0.6	H-2-Kb
1	1446	1454	KKQRNFDKI	0.61	H-2-Db
1	816	823	IQWNIRAF	0.62	H-2-Kb
1	283	291	NYHIFYQIL	0.62	H-2-Kb
1	1379	1388	TDAIQRTEEL	0.64	H-2-Db
1	124	131	TVNPYKWL	0.64	H-2-Kb
1	687	695	DNPLVMHQL	0.64	H-2-Kb
1	768	778	KAGLLGLLEEM	0.66	H-2-Db
1	289	299	QILSNKKPELL	0.66	H-2-Db
1	709	717	KGFPNRILY	0.67	H-2-Db
1	487	494	QQFFNHHM	0.68	H-2-Db
1	1643	1652	KHLKNSQAHL	0.68	H-2-Db
1	599	607	KDPLNETW	0.69	H-2-Db
1	486	494	LQQFFNHHM	0.69	H-2-Kb
1	532	540	MSILEEECM	0.7	H-2-Db
1	69	77	VTIKEDQVM	0.7	H-2-Db
1	1201	1209	SVAELGEQI	0.71	H-2-Db
1	1380	1388	DAIQRTEEL	0.72	H-2-Db
1	1488	1497	NAYEESLEHL	0.72	H-2-Db
1	190	198	RVIQYFASI	0.72	H-2-Db
1	1649	1657	QAHLKDTQL	0.72	H-2-Db
1	1723	1732	TSLINQKKKM	0.72	H-2-Db
1	1437	1444	SNAAAAAL	0.72	H-2-Kb
1	597	607	KNKDPINETW	0.73	H-2-Db
1	1328	1335	KNALAHAL	0.73	H-2-Kb
1	1675	1682	IVERRNNL	0.73	H-2-Kb
1	1757	1767	AKKAITDAAMM	0.75	H-2-Db

Seq#	Peptide start	Peptide end	Peptide	Percentile rank	Allele
1	642	649	KGSSFQTV	0.75	H-2-Kb
1	479	489	INFTNEKLQQF	0.76	H-2-Kb
1	550	558	KAKLYDNHL	0.76	H-2-Kb
1	1764	1771	AAMMAEEL	0.77	H-2-Db
1	645	652	SFQTVSAL	0.78	H-2-Kb
1	244	251	RFGKFIRI	0.79	H-2-Kb
1	514	522	FGMDLQACI	0.8	H-2-Db
1	763	771	TKVFFKAGL	0.8	H-2-Kb
1	544	553	ASDMTFKAKL	0.8	H-2-Kb
1	426	436	GALAKSVYEKM	0.81	H-2-Db
1	1830	1839	AEQKRNAESV	0.82	H-2-Db
1	1562	1570	RAQLEFNQI	0.82	H-2-Db
1	1519	1528	GEGGKNVHEL	0.83	H-2-Db
1	824	834	MGVKNWPWMKL	0.84	H-2-Db
1	157	165	ISDNAYQYM	0.85	H-2-Db
1	488	495	QFFNHHMF	0.85	H-2-Kb
1	769	778	AGILGLIEEM	0.86	H-2-Db
1	282	290	RNYHIFYQI	0.87	H-2-Db
1	485	495	KLQQFFNHHMF	0.88	H-2-Db
1	1157	1165	GATSVQIEM	0.89	H-2-Db
1	467	477	EIFDFNSFEQl	0.89	H-2-Kb
1	822	832	AFMGVKNWPWM	0.9	H-2-Db
1	332	340	ATDSAFDVL	0.9	H-2-Db
1	469	477	FDFNSFEQL	0.9	H-2-Db
1	428	436	LAKSVYEKM	0.91	H-2-Kb
1	651	660	ALHRENLNKl	0.92	H-2-Db
1	1102	1110	LALQLQKKL	0.94	H-2-Kb
1	667	674	THPHFVRC	0.94	H-2-Kb
1	260	268	ASADIETYL	0.94	H-2-Kb
1	644	651	SSFQTVSA	0.95	H-2-Kb
1	1679	1687	RNNLLQAEL	0.95	H-2-Kb
1	267	275	YLLEKSRVI	0.96	H-2-Db
1	283	290	NYHIFYQI	0.96	H-2-Kb
1	468	477	IFDFNSFEQL	0.97	H-2-Kb
1	1551	1561	ASLEHEEGKIL	0.98	H-2-Db
1	1301	1308	SQLTRGKL	0.98	H-2-Kb
1	1102	1110	LALQLQKKL	0.99	H-2-Db
1	667	675	THPHFVRCI	0.99	H-2-Kb

Extended Data Table 3.

HLA types for healthy donors and ICI-MC patients.

Subject Identifier	HLA-A Condensed/ Putative Allele Result	HLA-B Condensed/ Putative Allele Result	HLA-C Condensed/ Putative Allele Result	HLA-DPB1 Condensed/ Putative Allele Result	HLA-DQA1 Condensed/ Putative Allele Result	HLA-DQB1 Condensed/ Putative Allele Result	HLA-DRB1 Condensed/ Putative Allele Result	HLA-DRB3 Condensed/ Putative Allele Result	HLA-DRB Conde Putat Allel Resu
Myocarditis Pt 1	03:01:01G + 24:02:01G	07:02:01G + 51:01:01G	01:02:01G + 07:02:01G	02:02:01G + 04:01:01G	01:02:01G + 05:01:01G	03:01:01i + 06:02:01i	11:01:01i + 15:01:01i	02:02:01i + NP	NP +
Myocarditis Pt 2	02:01:01G + 24:02:01G	39:06:02G + 40:02:01G	07:02:01G + 15:02:01G	03:01:01G + 06:01:01G	03:01:01G + 04:01:01G	03:01:01i + 04:02:01i	04:01:01i + 08:01:01i	NP + NP	01:01:0 NP
Myocarditis Pt 3	01:01:01G + 03:01:01G	07:02:01G + 08:01:01G	07:01:01G + 07:02:01G	03:01:01G + 04:01:01G	01:02:01G + 05:01:01G	02:01:01i + 06:02:01i	03:01:01i + 15:01:01i	01:01:02i + NP	NP +
Healthy Donor 1	03:01:01G + 23:01:01G	07:02:01G + 44:03:01G	04:01:01G + 07:02:01G	02:01:02G + 02:01:02G	01:02:01G + 02:01:02G	02:02:01i + 06:02:01i	07:01:011 + 15:01:01i	NP + NP	01:01:0 NP
Healthy Donor 2	02:06:01G + 30:01:01G	14:02:01G + 48:01:01G	08:02:01G + 08:03:01G	02:01:02G + 04:01:01G	01:01:01G + 03:01:01G	03:04:01i + 05:01:01i	01:02:01i + 04:03:01i	NP + NP	01:01:0 NP
Healthy Donor 3	03:01:01G + 66:01:01G	41:02:01G + 57:01:01G	06:02:01G + 17:01:01G	04:01:01G + 04:01:01G	01:02:01G + 05:01:01G	03:01:01i + 05:02:01i	13:03:01i + 16:01:01i	01:01:02i + NP	NP +

Supplementary Material

Refer to Web version on PubMed Central for supplementary material.

Acknowledgements

Data Availability.

Sequencing data have been deposited in the Gene Expression Omnibus (GEO) under accession number GSE213486. Source data are provided for all studies involving animals.

References

1. Wang DY, Salem J-EE, Cohen JV., et al. Fatal Toxic Effects Associated With Immune Checkpoint Inhibitors: A Systematic Review and Meta-analysis. JAMA Oncol. 2018;4(12):1721–1728. http://www.embase.com/search/results?subaction=viewrecord&from=export&id=L624011231. Accessed October 15, 2019. [PubMed: 30242316]

2. Wei SC, Meijers WC, Axelrod ML, et al. A Genetic Mouse Model Recapitulates Immune Checkpoint Inhibitor–Associated Myocarditis and Supports a Mechanism-Based Therapeutic Intervention. Cancer Discov. 2020;11(3):614–639. doi:10.1158/2159-8290.cd-20-0856 [PubMed: 33257470]

3. Lv H, Havari E, Pinto S, et al. Impaired thymic tolerance to α-myosin directs autoimmunity to the heart in mice and humans. J Clin Invest. 2011;121(4):1561–1573. doi:10.1172/JCI44583 [PubMed: 21436590]

4. Gabrielsen ISM, Helgeland H, Akselsen H, et al. Transcriptomes of antigen presenting cells in human thymus. PLoS One. 2019;14(7):e0218858. doi:10.1371/JOURNAL.PONE.0218858 [PubMed: 31261375]

5. Johnson DB, Balko JM, Compton ML, et al. Fulminant myocarditis with combination immune checkpoint blockade. N Engl J Med. 2016;375(18):1749–1755. doi:10.1056/NEJMoa1609214 [PubMed: 27806233]

6. Hu J-RR, Florido R, Lipson EJ, et al. Cardiovascular toxicities associated with immune checkpoint inhibitors. Cardiovasc Res. 2019;115(5):854. https://academic.oup.com/cardiovascres/advance-article/doi/10.1093/cvr/cvz026/5304411. Accessed March 4, 2019. [PubMed: 30715219]

7. Salem JE, Manouchehri A, Moey M, et al. Spectrum of cardiovascular toxicities of immune checkpoint inhibitors: A pharmacovigilance study. Lancet Oncol. 2018;19(12):1579. doi:10.1016/S1470-2045(18)30608-9 [PubMed: 30442497]

8. Moslehi J, Lichtman AH, Sharpe AH, Galluzzi L, Kitsis RN. Immune checkpoint inhibitor–associated myocarditis: manifestations and mechanisms. J Clin Invest. 2021;131(5). doi:10.1172/JCI145186

9. Zamami Y, Niimura T, Okada N, et al. Factors Associated With Immune Checkpoint Inhibitor–Related Myocarditis. JAMA Oncol. 2019;5(11):1635–1637. doi:10.1001/JAMAONCOL.2019.3113 [PubMed: 31436802]

10. Salem J-E, Allenbach Y, Vozy A, et al. Abatacept for Severe Immune Checkpoint Inhibitor–Associated Myocarditis. N Engl J Med. 2019;380(24):2377–2379. doi:10.1056/NEJMc1901677 [PubMed: 31189043]

11. Yang X, Bam M, Becker W, Nagarkatti PS, Nagarkatti M. Long Noncoding RNA AW112010 Promotes the Differentiation of Inflammatory T Cells by Suppressing IL-10 Expression through Histone Demethylation. J Immunol. 2020;205(4):987–993. doi:10.4049/jimmunol.2000330 [PubMed: 32690657]

12. Jackson R, Kroehling L, Khitun A, et al. The translation of non-canonical open reading frames controls mucosal immunity. Nature. 2018;564(7736):434–438. doi:10.1038/s41586-018-0794-7 [PubMed: 30542152]

13. Adamo L, Rocha-Resende C, Lin CY, et al. Myocardial B cells are a subset of circulating lymphocytes with delayed transit through the heart. JCI insight. 2020;5(3). doi:10.1172/JCI.INSIGHT.134700

14. Bönner F, Borg N, Burghoff S, Schrader J. Resident cardiac immune cells and expression of the ectonucleotidase enzymes CD39 and CD73 after ischemic injury. PLoS One. 2012;7(4). doi:10.1371/JOURNAL.PONE.0034730

15. Martini E, Kunderfranco P, Peano C, et al. Single-Cell Sequencing of Mouse Heart Immune Infiltrate in Pressure Overload-Driven Heart Failure Reveals Extent of Immune Activation. Circulation. 2019;140(25):2089–2107. doi:10.1161/CIRCULATIONAHA.119.041694 [PubMed: 31661975]

16. Li O, Zheng P, Liu Y. CD24 expression on T cells is required for optimal T cell proliferation in lymphopenic host. J Exp Med. 2004;200(8):1083–1089. doi:10.1084/JEM.20040779 [PubMed: 15477346]

17. Hubbe M, Altevogt P. Heat-stable antigen/CD24 on mouse T lymphocytes: evidence for a costimulatory function. Eur J Immunol. 1994;24(3):731–737. doi:10.1002/EJI.1830240336 [PubMed: 8125140]

18. Szabo PA, Miron M, Farber DL. Location, location, location: Tissue resident memory T cells in mice and humans. Sci Immunol. 2019;4(34). doi:10.1126/SCIIMMUNOL.AAS9673

19. Fonseca R, Burn TN, Gandolfo LC, et al. Runx3 drives a CD8+ T cell tissue residency program that is absent in CD4+ T cells. Nat Immunol 2022 238. 2022;23(8):1236–1245. doi:10.1038/s41590-022-01273-4

20. Zhang L, Zlotoff DA, Awadalla M, et al. Major adverse cardiovascular events and the timing and dose of corticosteroids in immune checkpoint inhibitor-associated myocarditis. Circulation. 2020;141(24):2031–2034. doi:10.1161/CIRCULATIONAHA.119.044703 [PubMed: 32539614]

21. Coutinho AE, Chapman KE. The anti-inflammatory and immunosuppressive effects of glucocorticoids, recent developments and mechanistic insights. Mol Cell Endocrinol. 2011;335(1):2. doi:10.1016/J.MCE.2010.04.005 [PubMed: 20398732]

22. Heather JM, Spindler MJ, Alonso MH, et al. Stitchr: stitching coding TCR nucleotide sequences from V/J/CDR3 information. Nucleic Acids Res. 2022;1(1256879):13–14. doi:10.1093/nar/gkac190

23. Rosskopf S, Leitner J, Paster W, et al. A Jurkat 76 based triple parameter reporter system to evaluate TCR functions and adoptive T cell strategies. Oncotarget. 2018;9(25):17608–17619. doi:10.18632/oncotarget.24807 [PubMed: 29707134]

24. Jutz S, Leitner J, Schmetterer K, et al. Assessment of costimulation and coinhibition in a triple parameter T cell reporter line: Simultaneous measurement of NF-κB, NFAT and AP-1. J Immunol Methods. 2016;430:10–20. doi:10.1016/j.jim.2016.01.007 [PubMed: 26780292]

25. Gil-Cruz C, Perez-Shibayama C, de Martin A, et al. Microbiota-derived peptide mimics drive lethal inflammatory cardiomyopathy. Science (80-). 2019;366(6467):881–886. doi:10.1126/science.aav3487

26. Massilamany C, Gangaplara A, Steffen D, Reddy J. Identification of novel mimicry epitopes for cardiac myosin heavy chain-α that induce autoimmune myocarditis in A/J mice. Cell Immunol. 2011;271(2):438–449. doi:10.1016/J.CELLIMM.2011.08.013 [PubMed: 21939961]

27. Meier SL, Satpathy AT, Wells DK. Bystander T cells in cancer immunology and therapy. Nat Cancer 2022 32. 2022;3(2):143–155. doi:10.1038/S43018-022-00335-8

28. Maurice NJ, McElrath MJ, Andersen-Nissen E, Frahm N, Prlic M. CXCR3 enables recruitment and site-specific bystander activation of memory CD8+ T cells. Nat Commun 2019 101. 2019;10(1):1–15. doi:10.1038/S41467-019-12980-2

29. Simoni Y, Becht E, Fehlings M, et al. Bystander CD8 + T cells are abundant and phenotypically distinct in human tumour infiltrates. Nature. 2018;557(7706):575–579. doi:10.1038/S41586-018-0130-2 [PubMed: 29769722]

30. Maurice NJ, Taber AK, Prlic M. The Ugly Duckling Turned to Swan: A Change in Perception of Bystander-Activated Memory CD8 T Cells. J Immunol. 2021;206(3):455–462. doi:10.4049/JIMMUNOL.2000937 [PubMed: 33468558]

31. Scheper W, Kelderman S, Fanchi LF, et al. Low and variable tumor reactivity of the intratumoral TCR repertoire in human cancers. Nat Med. 2019;25(1):89–94. doi:10.1038/S41591-018-0266-5 [PubMed: 30510250]

32. Paul S, Sidney J, Sette A, Peters B. TepiTool: A pipeline for computational prediction of T cell epitope candidates. Curr Protoc Immunol. 2016;2016:18.19.1–18.19.24. doi:10.1002/cpim.12

33. Falk K, Rotzschke O, Stevanovic S, Jung G, Rammenseet H-G. Allele-specific motifs revealed by sequencing of self-peptides eluted from MHC molecules. 1991.

34. Luoma AM, Suo S, Williams HL, et al. Molecular Pathways of Colon Inflammation Induced by Cancer Immunotherapy. Cell. 2020;0(0):1–17. doi:10.1016/j.cell.2020.06.001

35. Johnson DB, Nixon MJ, Wang Y, et al. Tumor-specific MHC-II expression drives a unique pattern of resistance to immunotherapy via LAG-3/FCRL6 engagement. JCI Insight. 2018;3(24). http://www.ncbi.nlm.nih.gov/pubmed/30568030. Accessed December 21, 2018.

36. Ji C, Roy MD, Golas J, et al. Myocarditis in cynomolgus monkeys following treatment with immune checkpoint inhibitors. Clin Cancer Res. 2019;25(15):4735–

4748. doi:10.1158/1078-0432.CCR-18-4083/74931/AM/MYOCARDITIS-IN-CYNOMOLGUS-MONKEYS-FOLLOWING [PubMed: 31085720]

37. Woo SR, Turnis ME, Goldberg MV., et al. Immune inhibitory molecules LAG-3 and PD-1 synergistically regulate T-cell function to promote tumoral immune escape. Cancer Res. 2012;72(4):917–927. doi:10.1158/0008-5472.CAN-11-1620 [PubMed: 22186141]

38. Okazaki T, Okazaki IM, Wang J, et al. PD-1 and LAG-3 inhibitory co-receptors act synergistically to prevent autoimmunity in mice. J Exp Med. 2011;208(2):395. doi:10.1084/JEM.20100466 [PubMed: 21300912]

39. Chowell D, Morris LGT, Grigg CM, et al. Patient HLA class I genotype influences cancer response to checkpoint blockade immunotherapy. Science (80-). 2018;359(6375):582–587. doi:10.1126/science.aao4572

40. Naranbhai V, Groha S, Braun DA, et al. HLA-A*03 and response to immune checkpoint blockade in cancer: an epidemiological biomarker study. Lancet Oncol. 2021;0(0). doi:10.1016/S1470-2045(21)00582-9

41. Correale P, Saladino RE, Giannarelli D, et al. HLA Expression Correlates to the Risk of Immune Checkpoint Inhibitor-Induced Pneumonitis. Cells. 2020;9(9). doi:10.3390/CELLS9091964

42. Hasan Ali O, Berner F, Bomze D, et al. Human leukocyte antigen variation is associated with adverse events of checkpoint inhibitors. Eur J Cancer. 2019;107:8–14. doi:10.1016/J.EJCA.2018.11.009 [PubMed: 30529903]

43. McCulloch JA, Davar D, Rodrigues RR, et al. Intestinal microbiota signatures of clinical response and immune-related adverse events in melanoma patients treated with anti-PD-1. Nat Med 2022. February 2022:1–12. doi:10.1038/s41591-022-01698-2

44. Andrews MC, Duong CPMM, Gopalakrishnan V, et al. Gut microbiota signatures are associated with toxicity to combined CTLA-4 and PD-1 blockade. 2021;27(8):1432–1441. https://www.nature.com/articles/s41591-021-01406-6. Accessed November 2, 2021.

45. Van der Borght K, Scott CL, Martens L, et al. Myocarditis Elicits Dendritic Cell and Monocyte Infiltration in the Heart and Self-Antigen Presentation by Conventional Type 2 Dendritic Cells. Front Immunol. 2018;9:2714. doi:10.3389/fimmu.2018.02714 [PubMed: 30524444]

46. Rieckmann M, Delgobo M, Gaal C, et al. Myocardial infarction triggers cardioprotective antigen-specific T helper cell responses. J Clin Invest. August 2019. doi:10.1172/jci123859

47. Lee JH, Kim TH, Park HE, et al. Myosin-primed tolerogenic dendritic cells ameliorate experimental autoimmune myocarditis. Cardiovasc Res. 2014;101(2):203–210. doi:10.1093/CVR/CVT246 [PubMed: 24189626]

48. Tajiri K, Imanaka-Yoshida K, Tsujimura Y, et al. A New Mouse Model of Chronic Myocarditis Induced by Recombinant Bacille Calmette-Guèrin Expressing a T-Cell Epitope of Cardiac Myosin Heavy Chain-α. Int J Mol Sci. 2021;22(2):1–16. doi:10.3390/IJMS22020794

49. Hua X, Hu G, Hu Q, et al. Single-Cell RNA Sequencing to Dissect the Immunological Network of Autoimmune Myocarditis. Circulation. May 2020. doi:10.1161/circulationaha.119.043545

50. Taylor JA, Havari E, McInerney MF, Bronson R, Wucherpfennig KW, Lipes MA. A Spontaneous Model for Autoimmune Myocarditis Using the Human MHC Molecule HLA-DQ8. J Immunol. 2004;172(4):2651–2658. doi:10.4049/jimmunol.172.4.2651 [PubMed: 14764740]

Methods only extended references

51. Mombaerts P, Iacomini J, Johnson RS, Herrup K, Tonegawa S, Papaioannou VE. RAG-1-deficient mice have no mature B and T lymphocytes. Cell. 1992;68(5):869–877. doi:10.1016/0092-8674(92)90030-G [PubMed: 1547488]

52. Satija R, Farrell JA, Gennert D, Schier AF, Regev A. Spatial reconstruction of single-cell gene expression data. 2015;33(5):495–502. doi:10.1038/nbt.3192

53. Butler A, Hoffman P, Smibert P, Papalexi E, Satija R. Integrating single-cell transcriptomic data across different conditions, technologies, and species. Nat Biotechnol. 2018;36(5):411–420. doi:10.1038/nbt.4096 [PubMed: 29608179]

54. Stuart T, Butler A, Hoffman P, et al. Comprehensive Integration of Single-Cell Data. Cell. 2019;177(7):1888–1902.e21. doi:10.1016/j.cell.2019.05.031 [PubMed: 31178118]

55. Heather JM, Spindler MJ, Alonso MH, et al. Stitchr: stitching coding TCR nucleotide sequences from V/J/CDR3 information. bioRxiv. December 2021:2021.12.20.473544. doi:10.1101/2021.12.20.473544

56. Wu Y, Borde M, Heissmeyer V, et al. FOXP3 controls regulatory T cell function through cooperation with NFAT. Cell. 2006;126(2):375–387. doi:10.1016/J.CELL.2006.05.042 [PubMed: 16873067]

57. Gao J, Aksoy BA, Dogrusoz U, et al. Integrative analysis of complex cancer genomics and clinical profiles using the cBioPortal. Sci Signal. 2013;6(269). doi:10.1126/SCISIGNAL.2004088

58. Cerami E, Gao J, Dogrusoz U, et al. The cBio cancer genomics portal: an open platform for exploring multidimensional cancer genomics data. Cancer Discov. 2012;2(5):401–404. doi:10.1158/2159-8290.CD-12-0095 [PubMed: 22588877]

59. Oh HM, Oh JM, Choi SC, et al. An efficient method for the rapid establishment of Epstein-Barr virus immortalization of human B lymphocytes. Cell Prolif. 2003;36(4):191–197. doi:10.1046/J.1365-2184.2003.00276.X [PubMed: 12950388]

60. Granato M, Santarelli R, Farina A, et al. Epstein-Barr Virus Blocks the Autophagic Flux and Appropriates the Autophagic Machinery To Enhance Viral Replication. J Virol. 2014;88(21):12715. doi:10.1128/JVI.02199-14 [PubMed: 25142602]

61. Wölfl M, Greenberg PD. Antigen-specific activation and cytokine-facilitated expansion of naive, human CD8+ T cells. Nat Protoc 2014 94. 2014;9(4):950–966. doi:10.1038/nprot.2014.064

62. Eberhardt CS, Kissick HT, Patel MR, et al. Functional HPV-specific PD-1+ stem-like CD8 T cells in head and neck cancer. Nat 2021 5977875. 2021;597(7875):279–284. doi:10.1038/s41586-021-03862-z

63. Oksanen J, Blanchet FG, Friendly M, et al. Package "vegan" Title Community Ecology Package Version 2.5-7. 2020.

64. Nazarov V, immunarch.bot, Rumynskiy E. immunarch: An R Package for Painless Bioinformatics Analysis of T-Cell and B-Cell Immune Repertoires. June 2020. doi:10.5281/ZENODO.3893991
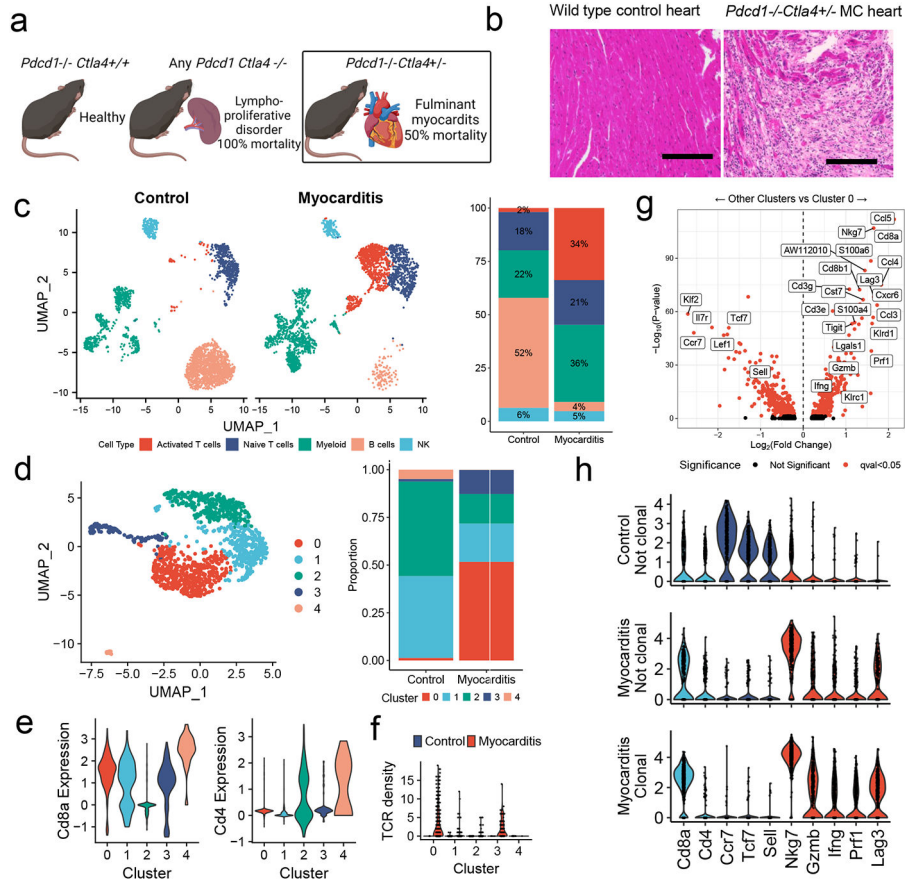
Figure 1. Single Cell RNA/TCR sequencing reveals abundant clonal effector CD8+ T cells in ICI-MC.

A) Phenotypic summary of mice with *Pdcd1* and *Ctla4* genetic loss. *Pdcd1−/−Ctla4+/+* mice do not have an overt phenotype. Mice with complete loss of *Ctla4* have a fatal lymphoproliferative disorder, regardless of *Pdcd1* genotype. *Pdcd1−/−Ctla4+/−* mice develop fulminant MC. B) H&E of cardiac tissue from a healthy wild type mouse and a *Pdcd1−/−Ctla4+/−* mouse with MC. Scale bar represents 200μm. Representative of n=10 animals per genotype. C) Dimensionality reduction with UMAP of scRNAseq on sorted CD45+ immune cells from control wild type mouse hearts (n=6) compared to hearts (n=4) of *Pdcd1−/−Ctla4+/−* mice with MC (n= 2509 cells per genotype). Cell type annotations were assisted by singleR and are quantified on the right. D) UMAP is subset on cells with *Cd3e* expression >1.5 and presence of a TCR, and then clustered using the Louvain algorithm (n=1266 cells). The proportion of the control and MC T cells in each cluster is quantified on the right. E) Expression of key T cell identity genes *Cd8a* and *Cd4* are shown for each T cell cluster. F) TCR density is a measure of how many of the 100 nearest neighbors share the same TCR α and β chain. TCR density is shown for each cluster and split by control or MC. G) Differential gene expression between cluster 0 T cells and all other T cell clusters (1,2,3, and 4). Higher expression in cluster 0 is indicated by positive fold change. Red indicates FDR-corrected p-value (q-value) <0.05. Black indicates not significant. h) Violin plots shown expression of key genes by clonality and sample. Clonal is defined as > 2 cells with the same TCR α and β chains. No clonal cells are seen in
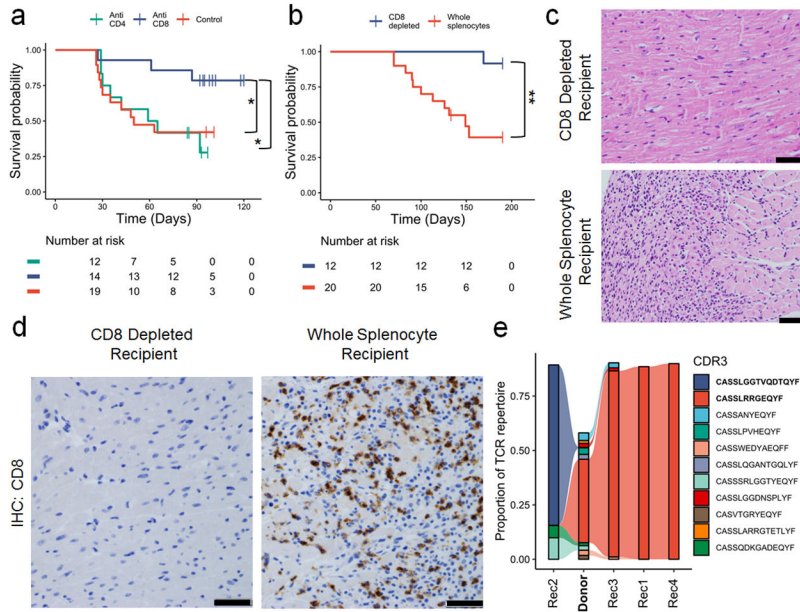
the control sample. Identity genes are light blue. Naïve T cells genes are dark blue. T cell activation genes are red.

Figure 2. CD8+ T cells are necessary for MC.

A) *Pdcd1−/−Ctla4+/−* mice were treated with anti-CD4, anti-CD8 or control antibodies. Antibody treatments were started at 21 days of age and administered three times weekly. Time is measured since birth, but no animals are censored prior to the start of the experiment at day 21. P =0.03, anti-CD8 v control, p=0.02, anti-CD8 v. anti-CD4, two-sided cox proportional hazard tests. Risk tables show size of groups. B) Whole splenocytes or splenocytes from which CD8 cells were depleted from *Pdcd1−/−Ctla4+/−* mice with MC were transferred to *Rag1−/−* recipient mice. Day 0 is the day of adoptive transfer. P=0.0017, two-sided cox proportional hazard test. Risk tables show size of groups. C) Representative H&E from CD8 depleted splenocyte recipients compared to whole splenocyte recipients. Only cardiac sections are shown. Scale bars show 50μm. Representative of n=10 animals per group. D) Representative IHC for CD8 on cardiac sections from CD8 depleted splenocyte recipients compared to whole splenocyte recipients. Scale bars show 50μm. Representative of n=10 animals per group. E) TCR β chain sequencing on cardiac tissue from a donor *Pdcd1−/−Ctla4+/−* mouse (Donor, in bold) and *Rag1−/−* whole splenocyte recipients (Rec1-4). The top ten most abundant TCRs from the donor plus the most abundant TCR from Rec2 are shown. Flow between samples indicates shared TCRs. Bolded CDR3s indicate most clonal TCRs.
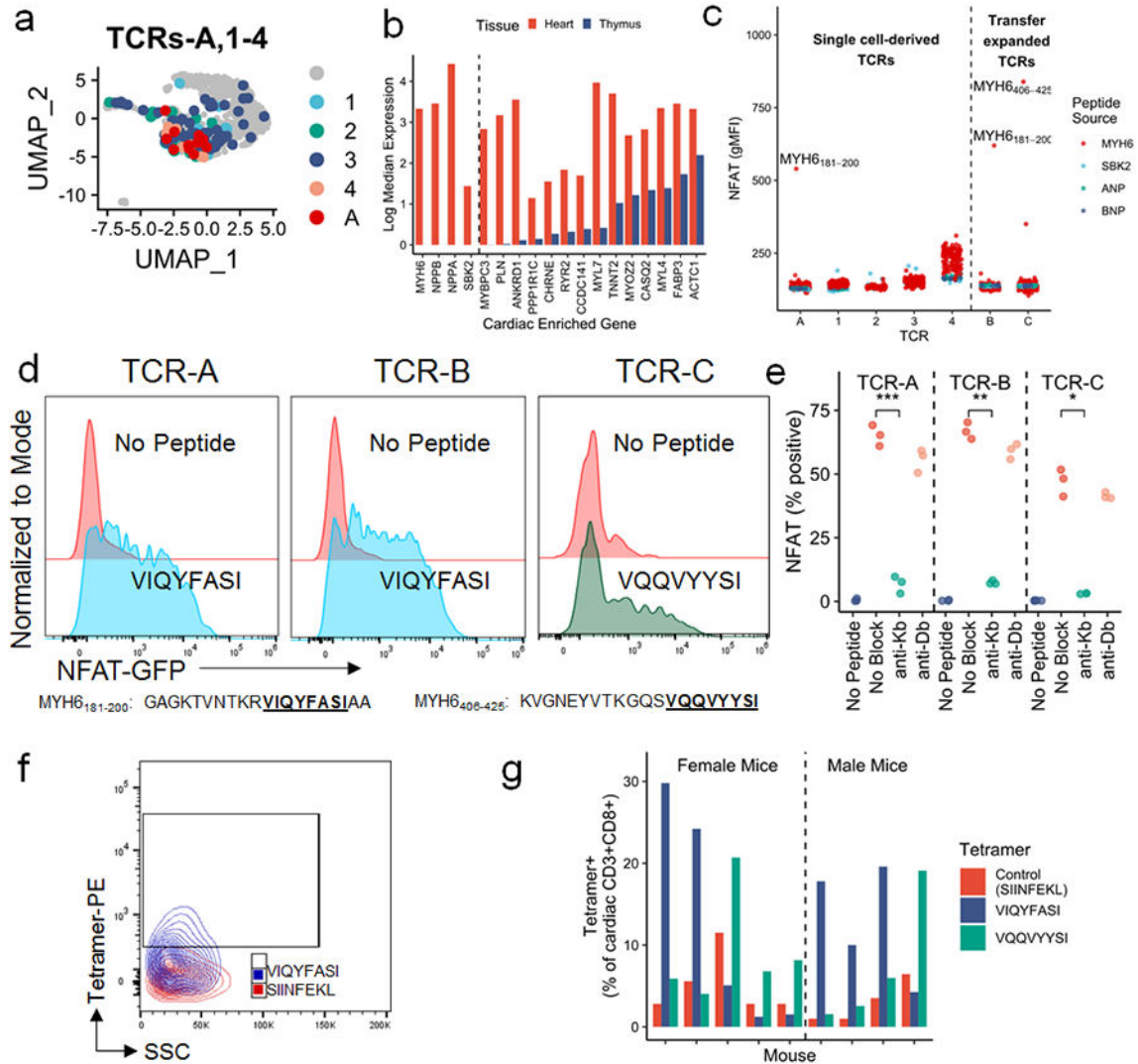
Figure 3. α-myosin is an MHC-I restricted autoantigen in murine MC.
A) TCRs-A, 1-4, used for antigen discovery, shown on the same plot as Fig. 1d. Grey cells do not express TCRs A or 1-4. b) Log median expression of 18 cardiac enriched genes in the heart (red) and thymus (blue). Genes to the left of the dashed line have no detectable expression in thymic APCs. c) NFAT-GFP reporter activity, measured by flow cytometry and shown as geometric mean fluorescence intensity, of all TCR cell lines stimulated independently with 172, 10-20aa SBK2, ANP, BNP, or α-myosin peptides. TCRs to the left of the dotted line are derived from single cell sequencing data (see Fig. 3a). TCRs to the right of the dotted line were selected due to expansion in adoptive transfer experiments (see Fig. 2e). TCRs named with letters (A-C) have a cognate antigen identified whereas TCRs named with numerals (1-4) do not have an identified cognate antigen. Top α-myosin peptide hits are labeled. d) Representative (of n=3 independent replicates) flow cytometry histograms of each TCR cell line co-cultured with BMDCs and stimulated with 10μg/mL predicted cognate peptide relative to no peptide. Peptide sequences are shown in the table. e) Each TCR cell line was co-cultured with EL-4 APCs and 10μg/mL cognate peptide (VIQYFASI for TCRs A and B; VQQVYYSI for TCR C; except for no peptide controls)

with or without 10μg/mL of anti-Kb or anti-Db blocking antibody. NFAT-GFP reporter activity is shown as percent of live cells. n=3 biological replicates. P=0.00035 (TCR-A), p=0.004 (TCR-B), p=0.013 (TCR-C), two-sided t-tests for no block to anti-Kb, adjusted for multiple comparisons. f) Representative flow cytometry of SIINFEKL (red) and VIQYFASI (blue) loaded H2-Kb tetramer staining on cardiac CD3+CD8+ cells. g) Quantification of control, VIQYFASI, and VQQVYYSI H2-Kb-tetramer staining in cardiac CD3+CD8+ cells in individual mice. Each group of three bars represents one mouse with MC. n=9 mice (n=5 female; n=4 male).
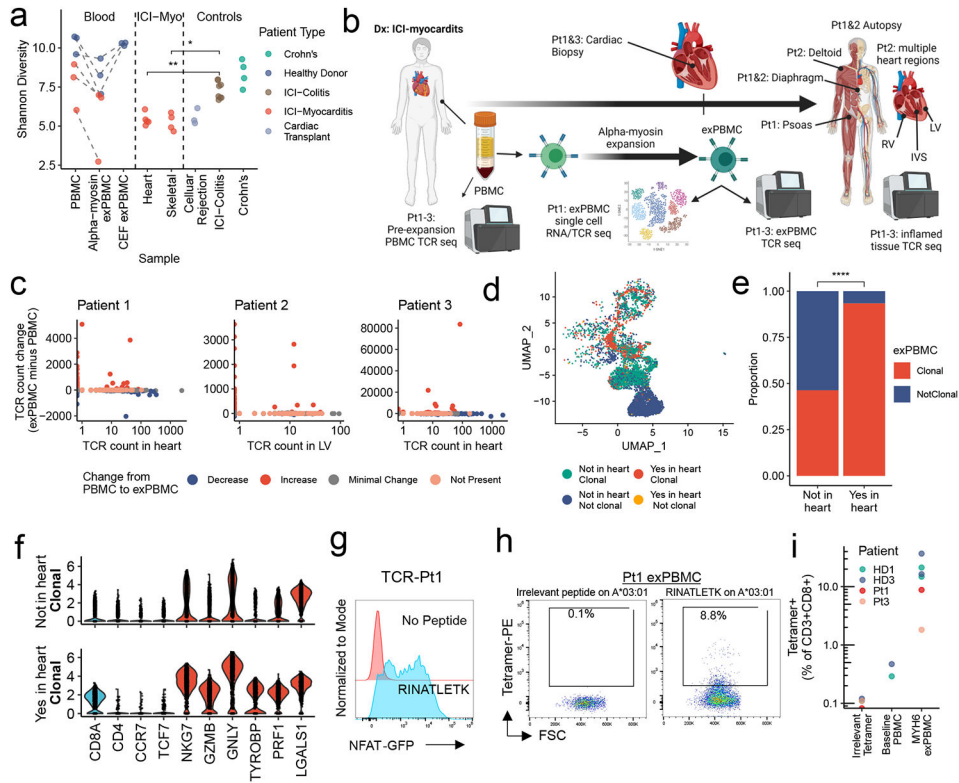
Figure 4. α-myosin expanded TCRs are present in cardiac and skeletal muscle of patients with ICI-MC.

a) Shannon diversity of TCR beta chain repertoires. Dashed lines connect blood samples within same donor. P-values represent two-sided Wilcoxon tests. n=6 PBMC, n= 6 α-myosin exPBMC, n=3 CEF exPBMC, n=5 heart from 3 patients (multiple regions for pt2), n=4 skeletal muscle from 2 patients, n=3 rejection from 3 cardiac transplant patients, n=8 ICI-colitis from 8 patients, n=4 Crohn's from 4 patients. b) ICI-MC patient tissues. RV= right ventricle. LV = left ventricle. IVS = interventricular septum. c) Change in TCR counts from PBMC to α-myosin exPBMC plotted by abundance of the same TCR beta chain in the autologous inflamed cardiac tissue. Minimal change is less than a 50 read count change. Not present means not found in either PBMC or exPBMC. d) Dimensionality reduction with UMAP on scRNAseq of CD3+ patient 1 exPBMC. Groups are divided by whether the TCR beta chain expressed by that cell is present in the patient's heart and whether that TCR is clonal (expressed by >2 cells in exPBMC). e) Proportion of single cell sequenced exPBMCs that are clonal, stratified by whether that TCR is present in the heart. P<0.0001 by two-sided Fisher's Exact test. f) Violin plots of key genes by presence or absence in heart and clonality in exPBMC. Identity genes are light blue. Naïve genes are dark blue. Activation genes are red. g) Flow cytometry histogram of TCR-Pt1 reporter cell line co-cultured with autologous LCLs and stimulated with 10μg/mL RINATLETK peptide relative to no peptide. (n=3 replicates) h) Scatter plot showing CD3+CD8+ Pt1 exPBMC stained with irrelevant peptide or RINATLETK on HLA-A:03*01 tetramer. i) Quantification of RINATLETK on HLA-A:03*01 tetramer staining across samples, compared to irrelevant peptide. n=2 healthy

donors for baseline PBMC. n=6 exPBMC (1 replicate for 2 ICI-MC patients and 2 replicates for 2 healthy donors).

Table 1.

Summary of TCR CDR3, V and J genes for TCRs used in antigen discovery experiments.

TCR ID	TCR Source	β CDR3	TRBV	TRBJ	α CDR3	TRAV	TRAJ	Antigen
A	Murine single cell sequencing	CSAAWGGSAETLYF	TRBV1	TRBJ2-3	CAVSDRGSALGRLHF	TRAV7-3*04	TRAJ18	MYH6$_{191-198}$ (VIQYFASI)
1	Murine single cell sequencing	CASSPGQGAYAEQFF	TRBV12-2	TRBJ2-1	CAVSSGYGSSGNKLIF	TRAV7-5	TRAJ32	Unknown (Not in α-myosin, SBK2, ANP, BNP)
2	Murine single cell sequencing	CASKTGYNYAEQFF	TRBV19	TRBJ2-1	CALNTGYQNFYF	TRAV4-4-DV10	TRAJ49	Unknown (Not in α-myosin, SBK2, ANP, BNP)
3	Murine single cell sequencing	CASGGLGGPSQNTLYF	TRBV12-2	TRBJ2-4	CALERSTGNYKYVF	TRAV13-1	TRAJ40	Unknown (Not in α-myosin, SBK2, ANP, BNP)
4	Murine single cell sequencing	CASSDAGYAEQFF	TRBV13-3	TRBJ2-1	CALGDSNYQLIW	TRAV6-6	TRAJ33	Unknown (Not in α-myosin, SBK2, ANP, BNP)
B	Adoptive transfer (Donor, Rec1,3,4)	CASSLRRGEQYF	TRBV15	TRBJ2-7	CALERASGSWQLIF	TRAV13-1	TRAJ22	MYH6$_{191-198}$ (VIQYFASI)
C	Adoptive Transfer (Rec2)	CASSLGGTVQDTQYF	TRBV12-2	TRBJ2-5	CALGDRNNAGAKLTF	TRAV6D-6	TRAJ39	MYH6$_{418-425}$ (VQQVYYSI)
TCR_pt1	Pt 1 exPBMC (single cell sequencing)	CASSPYQSSGANVLTF	TRBV9	TRBJ2-6	CALSDRYGGATNKLIF	TRAV19	TRAJ32	MYH6$_{443-451}$ (RINATLETK)

Table 2.

Summary of MC patient information.

Pt	Age	Sex	ICI history	Primary Tumor	Disease tissue TCR sequencing	Brief Clinical Course
1	75	M	Ipilimumab + Nivolumab	Renal cell carcinoma	Cardiac biopsy; Autopsy: diaphragm, psoas	Pt 1 presented to the emergency department with chest pain 3wks post initiation of ICI and was found to have ventricular tachycardia (VT), and elevated troponin. EMB confirmed MC. Pt's clinical course was complicated by cardiogenic shock, acute hypoxic respiratory failure and acute renal failure, despite high dose steroids. The pt and family declined further aggressive treatment with curative intent and opted for palliative extubation.
2	64	M	Nivolumab	Small cell lung cancer	Autopsy: RV, LV, IVS, deltoid, diaphragm	Pt2 was admitted to the hospital with recurrent VT and elevated troponin. Pt was found to have a dilated RV on echo. Prednisone treatment with initiated. EMB was complicated by RV perforation leading to acute cardiac tamponade, left atrial thrombus, and rapid clinical deterioration. Family opted for palliative extubation.
3	78	M	Pembrolizumab	Lung adenocarcinoma	Cardiac biopsy	Pt3 was evaluated for fatigue and myalgias and was found to have elevated troponin. The patient was admitted, started on high dose steroids and MC was confirmed by EMB. Patient recovered with steroid treatment and did not experience recurrence of MC. The patient died 5 months later in home hospice due to complications related to a hemothorax which was potentially related to underlying malignancy.